Quaternary Science Reviews 250 (2020) 106645

Contents lists available at ScienceDirect

Quaternary Science Reviews

journal homepage: www.elsevier.com/locate/quascirev

Rapid retreat of a Scandinavian marine outlet glacier in response to warming at the last glacial termination

Henning Åkesson [a, b, *], Richard Gyllencreutz [b], Jan Mangerud [a], John Inge Svendsen [a], Faezeh M. Nick [c], Kerim H. Nisancioglu [a, d]

[a] Department of Earth Science, University of Bergen and Bjerknes Centre for Climate Research, Bergen, Norway
[b] Department of Geological Sciences and Bolin Centre for Climate Research, Stockholm University, Stockholm, Sweden
[c] Department of Arctic Geology, University Centre in Svalbard, Longyearbyen, Norway
[d] Centre for Earth Evolution and Dynamics, University of Oslo, Oslo, Norway

ARTICLE INFO

Article history:
Received 21 January 2020
Received in revised form
23 September 2020
Accepted 9 October 2020
Available online 10 November 2020

Keywords:
Modeling
Deglaciation
Glacier
Marine-terminating glaciers
Younger dryas
Scandinavian ice sheet

ABSTRACT

Marine outlet glaciers on Greenland are retreating, yet it is unclear if the recent fast retreat will persist, and how atmosphere and ocean warming will impact future retreat. We show how a marine outlet glacier in Hardangerfjorden retreated rapidly in response to the abrupt warming following the Younger Dryas cold period (approximately 11,600 years before present). This almost 1000 m deep fjord, with several sills at 300–500 m depth, hosted a 175 km long outlet glacier at the western rim of the Scandinavian Ice Sheet. We use a dynamic ice-flow model constrained by well-dated terminal and lateral moraines to simulate the reconstructed 500-year retreat of Hardangerfjorden glacier. The model includes an idealized oceanic and atmospheric forcing based on reconstructions, but excludes the surface mass balance-elevation feedback. Our simulations show a highly episodic retreat driven by surface melt and warming fjord waters, paced by the fjord bathymetry. Warming air and ocean temperatures by 4–5 °C during the period of retreat result in a 125-km retreat of Hardangerfjorden glacier in 500 years. Retreat rates throughout the deglaciation vary by an order of magnitude from 50 to 2500 m a^{-1}, generally close to 200 m a^{-1}, punctuated by brief events of swift retreat exceeding 500 m a^{-1}, each event lasting a few decades. We show that the fastest retreat rates occur in regions of the bed with the largest retrograde slopes; ice shelf length and fjord water depth is less important. Our results have implications for modern glacial fjord settings similar to Hardangerfjorden, where high retreat rates have been observed. Our findings imply that increasing air temperatures and warming subsurface waters in Greenland fjords will continue to drive extensive retreat of marine outlet glaciers. However, the recent high retreat rates are not expected to be sustained for longer than a few decades due to constraints by the fjord bathymetry.

1. Introduction

Our capacity to predict future sea level rise from outlet glacier discharge is largely based on short observational records from ice sheets and ice caps (e.g. Howat et al., 2005; Luckman et al., 2006; Moon et al., 2012; Ritz et al., 2015; Nias et al., 2019). While these data are vital for process understanding, they cannot reconcile responses to climate change beyond a few decades. In contrast, geological reconstructions of former ice sheets offer invaluable information on long-term outlet glacier behavior and their climatic controls (Briner et al., 2009; Young et al., 2011; Hughes et al., 2012; Mangerud et al., 2013, 2019; Stokes et al., 2014). Still, the temporal resolution of the provided retreat rates is limited by the available geological data. Due to these limitations of the observational records and geological reconstructions, the potential duration and maximum rates of retreat of marine outlet glaciers are poorly known.

Externally forced mass loss for marine outlet glaciers can be caused by either oceanic or atmospheric warming (e.g. Catania et al., 2020). Mass loss in response to warming ocean water causes frontal ablation, which can be divided into direct submarine melting of the calving front and iceberg calving. Alternatively, atmospheric warming may remove ice mass either directly through

* Corresponding author. Department of Geological Sciences and Bolin Centre for Climate Research, Stockholm University, Stockholm, Sweden.
E-mail address: henning.akesson@geo.su.se (H. Åkesson).

https://doi.org/10.1016/j.quascirev.2020.106645

surface melt, or indirectly through enhanced surface runoff, which in turn increases subglacial discharge, causing more vigorous melting at the submarine calving front (e.g. Jenkins, 2011).

A leading hypothesis for Greenland is that incursions of warm subsurface ocean water onto the shelves and into the fjords triggered the recent outlet glacier retreat (Holland et al., 2008; Murray et al., 2010; Straneo and Heimbach, 2013). However, it is not established whether warming ocean waters or surface air temperatures will be the main driver of mass loss on multi-decadal to centennial timescales (Slater et al., 2019; Aschwanden et al., 2019). Through numerical model experiments on multi-decadal timescales, Morlighem et al. (2019) found that outlet glaciers in northwest Greenland were more sensitive to ocean warming than to increased subglacial discharge caused by atmospheric warming. In contrast, mass loss caused by atmospheric warming, rather than increased outlet glacier discharge, may dominate Greenland's contribution to sea level over the next centuries to millennium (Aschwanden et al., 2019).

To put the recent outlet glacier behavior into perspective, we use a dynamic ice-flow model (Vieli et al., 2001; Nick et al., 2013) to simulate a continuous, multi-century collapse of the Hardangerfjorden glacier in response to climate and ocean warming at the last glacial termination. We aim to assess the drivers and transient dynamics of the data-constrained 500-year retreat from the fjord mouth to the fjord head. An ensemble of model experiments with different model parameters and forcings is used to investigate the sensitivity to atmospheric and ocean forcing, as well as to iceberg calving. The model is able to reproduce the reconstructed rapid retreat within dating uncertainties, and the ensemble approach allows us to identify the probable forcing mechanism(s) and the most likely retreat scenario.

Similar topography and climatic settings make this marine outlet glacier in western Norway a close analogue to the modern-day Jakobshavn Isbræ and similar outlet glaciers on Greenland (Mangerud et al., 2013; Åkesson et al., 2018a,b; see section 6.3). The retreat of the Hardangerfjorden glacier during the Early Holocene is exceptionally well-dated, as described in section 2.2. We also know from lake sediment core data that offshore warm water likely entered Hardangerfjorden during deglaciation (Romundset et al., 2010; see Section 4.4). Unlike studies of present-day glaciers in Greenland, the ice-free landscape of Norway (Fig. 1) provides a highly detailed bed topography for the model experiments.

2. Study area and empirical constraints

2.1. Bathymetry and bedrock topography

A digital terrain model of the drainage basin and surrounding fjord areas was compiled at 500 m resolution by merging topographic and bathymetric data from the Norwegian Mapping Authority (Kartverket, 2017). The bathymetric point data was gridded using a distance weighted average algorithm. Present-day ice caps were removed to derive our bed topography, by subtracting published ice thickness data (Førre, 2012; Åkesson et al., 2017, Fig. 2a and b). We also account for post-glacial rebound using an uplift gradient of 1.3 m km^{-1} along the flowline, based on shoreline diagrams for the Younger Dryas (Mangerud et al., 2013).

The constructed glacier flowline follows the deepest part of the fjord (Fig. 2a), although glacier striae show that the glacier made some 'short-cuts' relative to the winding deepest part of the channel (Holtedahl, 1975). These short-cuts are located where the fjord winds back and forth (Fig. 2a), for example out of Sørfjorden (~km 65 along the flowline), at Jondal (~km 110) and the island Varaldsøy at ~ km 120 (see Fig. 2a and b). These short-cuts are not taken into account in the modeling, but given the spatial resolution of the model and the underlying data (500 m), and the simplicity of the model (width- and depth-averaged, Sect. 3.1), the model would not capture such short-cuts anyway. In reality, these winding sections of the fjord may slow down retreat slightly due to the topographic hindrances they represent, but we do not expect that this affects the main retreat pattern. Geometric constraints for the model were extracted by sampling bed elevation at 500 m intervals in the 500-m composite digital elevation model (DEM) along the flowline, and along cross-profiles perpendicular to the flowline. In the model, fjord bathymetry and ice surface data are smoothed using a 5 km low-pass moving average filter of the 500-m topography to ensure numerical stability (Fig. 3a).

Recent studies suggest that variations in lateral topography, in addition to bedrock variations, may be important for the stability of marine outlet glaciers (Jamieson et al., 2012; Stokes et al., 2014; Steiger et al., 2018; Åkesson et al., 2018a,b). To better capture such effects, we defined four cross-flow zones from the central flowline (Fig. 2c) and calculated cross-sectional bedrock slopes using a linear regression within each zone.

Post-glacial sediments in the fjord are evenly distributed, except on local bedrock highs, where it is thinner (Aarseth, 2004). We measured the sediment thickness in 23 locations of Fig. 12 of Aarseth et al. (1997), which is an interpreted seismic line along the entire Hardangerfjorden. The thickness varied between 47 and 190 m, with an average of 105 m and a median of 101 m. The bathymetry along the flowline was therefore corrected for postglacial sediments by subtracting 100 m from the bed elevation. We assume that the glacier rested on bedrock with a negligible sediment cover (Aarseth et al., 1997). The bedrock in the area consists of crystalline rocks giving strong seismic contrast to the marine sediments. The estimates of sediments thicknesses are therefore considered to have a precision well inside other uncertainties.

2.2. Reconstruction of the ice-margin retreat from geological observations

The empirical background for the present paper is Mangerud et al. (2013), where the moraines and numerical dates are described in detail. There are two main moraine systems in the Hardangerfjorden region, which are used for the reconstruction. The oldest is the Herdla-Halsnøy Moraine (Fig. 1b), which crosses the mouth of the fjord along the island Halsnøy, formed by a major glacial re-advance during the Younger Dryas, documented by about 40 radiocarbon dates of shell fragments incorporated in the till (Mangerud et al., 2016). The start of retreat from the moraine is dated to 11.6 ± 0.1 cal ka BP by a sequence of 15 radiocarbon dates of terrestrial plant macrofossils across the transition from glacial silt to organic sediments in a basin located just outside the moraine (Lohne et al., 2012; Mangerud et al., 2013). The end moraine continues as a distinct, up to 10–15 m high, lateral moraine that can be traced up to a height of 1000 m a.s.l. along the south side of the fjord (Follestad, 1972) and dated by ^{10}Be exposure dates (Mangerud et al., 2013). This moraine system constrains the extent and thickness of the fjord glacier at the end of the Younger Dryas (Fig. 3a).

The youngest moraine system, the Eidfjord-Osa Moraine, is marked by distinct moraine lobes that can be traced from the mountain plateau down the steep valleys to the head of Hardangerfjorden (Anundsen and Simonsen, 1967), where a prominent glaciomarine delta (105 m a.s.l.) was deposited at the village Eidfjord during a re-advance (cf. Fig. 3a). The final deglaciation of the fjord is best dated to 11.1 ± 0.1 ka based on dating of the oldest shoreline near the fjord head and supported by 15 ^{10}Be exposure ages from the Eidfjord-Osa Moraine, giving a mean age of 11.07 ± 0.31 ka (Mangerud et al., 2013). Results from several radiocarbon dates from coring of isolation basins in the mid-fjord

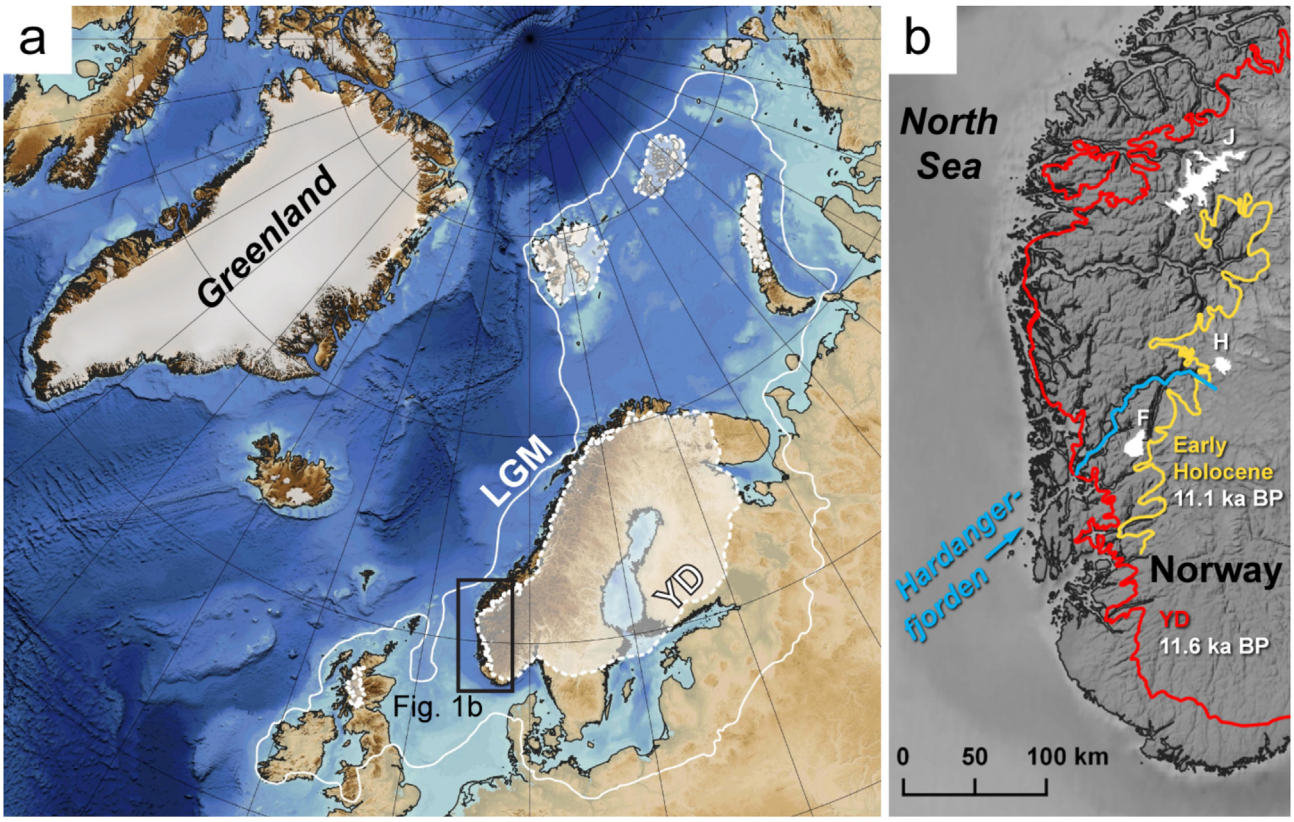

Fig. 1. (a) Location of the study area and the LGM (21 ka BP) and Younger Dryas (12 ka BP) ice margins of the Eurasian Ice Sheet (Hughes et al., 2016); (b) Location of Hardangerfjorden in relation to the Late Younger Dryas (11.6 ka BP) and Early Holocene (11.1 ka BP) ice margins in southwestern Norway. The model flowline is depicted in blue. White areas denote present-day ice caps: J - Jostedalsbreen, H - Hardangerjøkulen, F- Folgefonna. (For interpretation of the references to color in this figure legend, the reader is referred to the Web version of this article.)

region suggest that this part became ice free 11.3 ± 0.1 ka BP (Romundset et al., 2010), consistent with the ages from the mouth and head of the fjord.

The distance between the Halsnøy and Eidfjord moraines is about 120 km and, according to the given ages, the retreat took 500 ± 140 years, giving a mean retreat rate of 240 ± 70 m yr^{-1}.

2.3. Climate during the Younger Dryas – Holocene transition

Fossil ice wedges indicate permafrost during (at least parts of) the YD in western Norway (Mangerud, 1987), implying mean annual air temperatures below −1 °C (Brown, 1960). At the YD–Holocene transition, the air temperature rose by several degrees in a few decades in Norway (Birks et al., 2000, 2005; Bjune et al., 2005), as well as on Greenland (Steffensen et al., 2008; Simonsen et al., 2011), with a somewhat larger temperature change in the Norwegian Sea (Eldevik et al., 2014).

Since summer temperature, and particularly winter precipitation estimates, for the YD-Holocene transition are not well constrained, we represent the change in climate by a change in the equilibrium line altitude (ELA). The YD ELA is reconstructed to 880 m a.s.l. near the middle of the Hardangerfjord, based on reconstructions from nearby local ice caps and the highest extent of lateral moraines, corrected for Holocene bedrock uplift (Mangerud et al., 2013, 2016). ELA estimates for the YD are based on the assumption that lateral moraines do not form above the ELA (Lichtenecker, 1936; Andrews, 1975). The YD ELA at 880 m a.s.l. is a minimum estimate since the highest lateral moraines may form some distance downstream from the ELA (Benn and Lehmkuhl, 2000), but our reconstructed ELA is considered fairly reliable in light of the prominent moraines that can be traced from sea level up to the uplands around Hardangerfjorden (Andersen, 1954; Follestad, 1972).

Given the rapid climate warming documented for the YD-Holocene transition, we impose a stepwise change of the model ELA, which is further detailed in Section 4.2. For context, the present ELA at the Folgefonna ice cap, at the southern rim of the Hardangerfjorden, is 1340–1520 m a.s.l. (Andreassen et al., 2005; Mangerud et al., 2016, Fig. 3a).

2.4. Sea level change and the deglaciation of Norway

Over the centennial time scales we consider, sea level changes have the potential to slow down or amplify retreat due to their influence on flotation and calving of marine-based termini. However, we can rule out rising sea level as an amplifying n factor of the rapid retreat of Hardangerfjorden glacier in the early Holocene: relative sea level was falling at rates of c. 7 and 20 m per 100 years at Halsnøy and Eidfjord, respectively, as the bedrock rebounded in response to the loss of the overlying ice load, and because of a weaker gravitational attraction of the ocean by the smaller ice mass (Mangerud et al., 2013). If anything, sea level must have been a dampening factor on the retreat, as has been suggested by idealized modeling (Gomez et al., 2010).

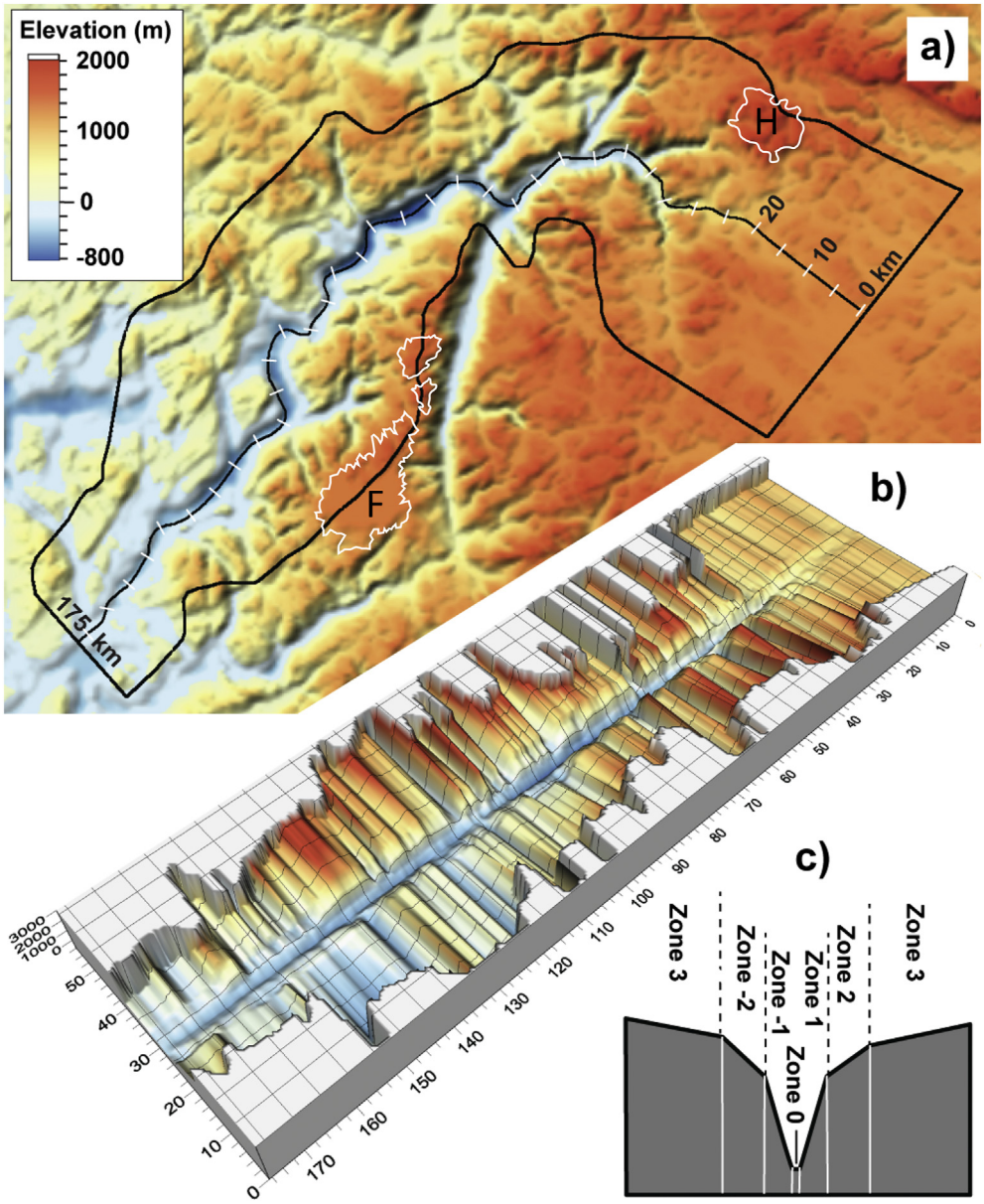

Fig. 2. (a) Topography in the model domain, where white outlines denote present-day ice caps F - Folgefonna (three ice caps) and H - Hardangerjøkulen based on the GLIMS database (Raup et al., 2007), (b) model representation of the topography, (c) cross-sectional view of how the lateral model topography is constructed, using zones of varying width from the flowline, with linearly regressed slopes for each zone. The zones are as follows. Zone 0: Central flowline ±250 m (total width = 500 m), postulated to be flat in cross-profile. Zone 1: 250–1750 m from central flowline (width 1.5 km), covering the central deep trough (mostly below sea level). Zone 2: 1750–4250 m from central flowline (width 2.5 km), where bedrock topography clearly slopes towards the flowline. Zone 3: 4250 m–drainage boundary, marking the outer zone that on average slopes towards the fjord, but locally differs.

3. Model description

3.1. Ice dynamics

We use a vertically and horizontally integrated flowline model (Vieli et al., 2001; Vieli and Payne, 2005; Nick et al., 2010, 2013) accounting for the full balance of driving and resistive stresses. The model derivation is detailed in Nick et al. (2010). Only the momentum balance is described here:

$$\rho_i g H \frac{\partial h}{\partial x} = 2\frac{\partial}{\partial x}\left(H\nu\frac{\partial U}{\partial x}\right) - \beta U^{\frac{1}{m}} - \frac{2H}{W}\left(\frac{5U}{AW}\right)^{\frac{1}{n}}, \quad (1)$$

where h is the surface elevation, H is ice thickness, U is the depth- and width-integrated ice velocity, ρ_w and ρ_i are seawater and ice density, respectively, $n = 3$ is the exponent in Glen's flow law and g is the gravitational acceleration. Note that the lateral drag (the third term on the right-hand side in Eq. (1)) is parameterized as a function of the channel-width W and the ice viscosity A (Van der Veen and Whillans, 1996), and any floating ice is able to buttress upstream ice (Nick et al., 2009; Vieli and Nick, 2011). As described in detail in Section 3.2, W is the cross-sectional width measured at the intersection between the ice surface and the fjord walls. The effective viscosity ν depends non-linearly on the effective strain rate (Paterson, 1994), and we assume a non-linear Weertman-type sliding law with $m = 3$ (Weertman, 1964; Fowler, 2010). It is not obvious which sliding law is most appropriate for a given glacier,

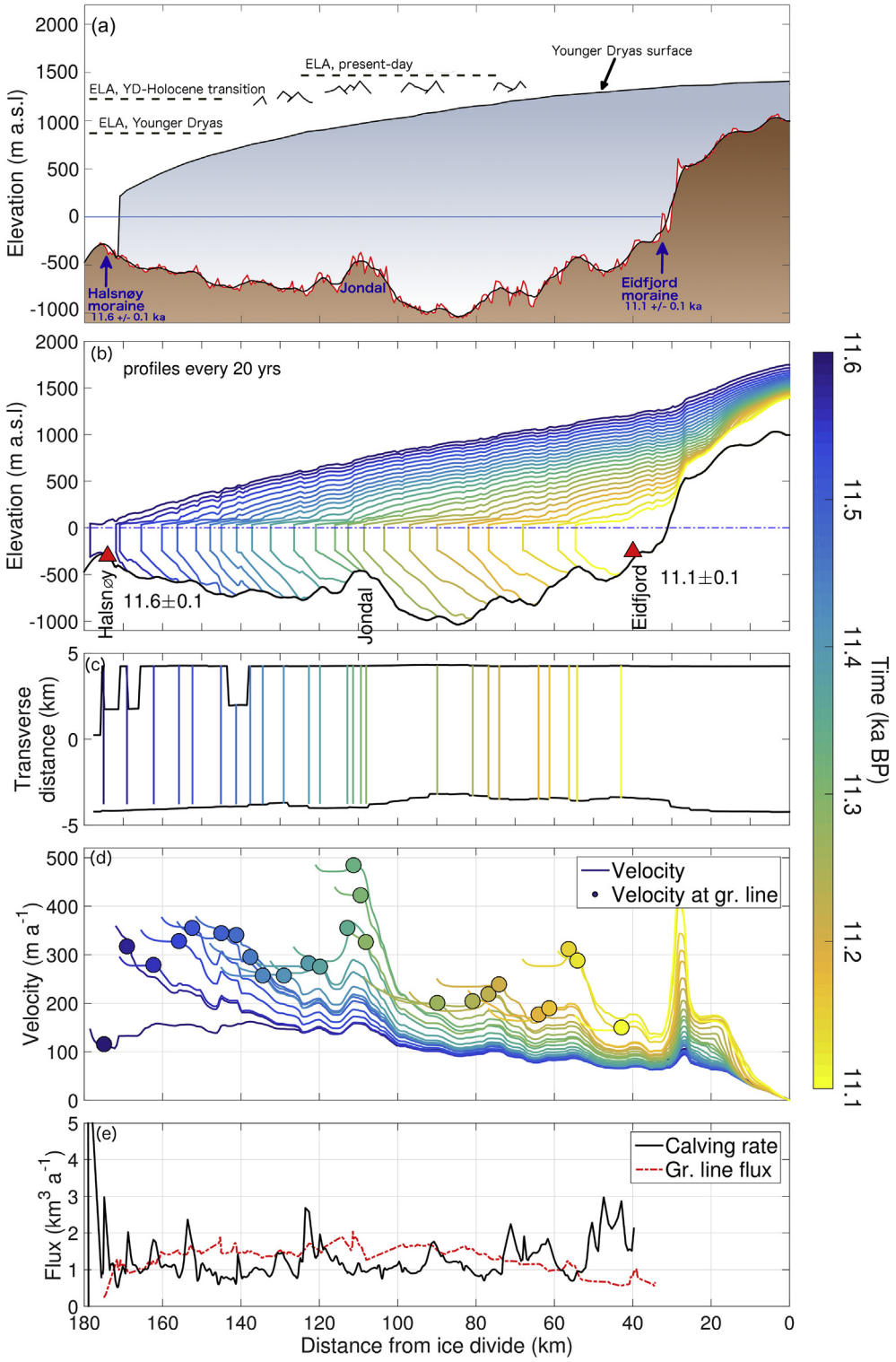

Fig. 3. Retreat of Hardangerfjorden glacier at the end of the last glacial. (a) Along-flow Younger Dryas surface (Mangerud et al., 2013) and observed and smoothed bedrock topography (data from Norwegian Mapping Authority). Mountain peaks along the fjord are shown schematically. Postglacial sediments are removed and bed topography is corrected for postglacial uplift. The ELA for the YD-Holocene transition is based on the 'best-guess' model simulation, while the ELAs for the Younger Dryas and present-day are based on reconstructions and observations, respectively. (b) Modelled geometry of Hardangerfjorden glacier during the retreat 11.6–11.1 ka BP, with dated moraines at Halsnøy and Eidfjord. Model profiles are shown every 20 years. (c) Modelled planview grounding lines, (d) velocity along the flowline and at the grounding line, (e) calving rate and grounding line flux.

yet the choice of sliding law may influence grounding line dynamics (e.g. Brondex et al., 2017). Here we have assumed a similar representation of sliding (Sect. 3.2) that previously has been shown to work well for this flowline model (Nick et al., 2010, 2013; Steiger et al., 2018).

As the flowline model is depth- and width-averaged it is computationally efficient, which allows for an extensive ensemble study exploring the factors important to the simulated retreat. The model can, however, not resolve across-flow variations in topography within our across-flow zones described in Section 2.1. Nevertheless, Hardangerfjorden is a relatively simple fjord system (Fig. 1b) and we consider the model suitable as applied in this study. Our ice divide is estimated based on the pattern of glacial striae and the present-day water divide, which if placed incorrectly will affect upstream fluxes from the interior.

3.2. Parameters and grounding line treatment

We assume isothermal, isotropic ice with a uniform ice viscosity A, corresponding to an ice temperature $T_{ice} = -5$ °C (Cuffey and Paterson, 2010, p.75), consistent with present-day western Greenland (Luthi et al., 2002), an area of similar maritime climate as expected for southwestern Norway at the YD–Holocene transition.

For basal motion, we construct a uniform slippery basal drag coefficient $\beta = 8000$ Pa m$^{-2/3}$ s$^{-1/3}$ in Eq. (1) below sea level, and more sticky ($\beta = 22{,}000$ Pa m$^{-1/3}$ s$^{-1/3}$) for areas of the bed above sea level. These values are not well constrained and are chosen based on a study of present-day Greenland outlet glaciers (Nick et al., 2013), which we believe is an appropriate climatic and topographic analogue for Hardangerfjorden at the YD-Holocene transition. As ice thickness and resulting effective pressure decreases towards the grounding line, the basal shear stress approaches zero, and is set to zero for floating ice. We refrain from imposing ad-hoc variations of basal friction through time. The current poor understanding of the interannual evolution of glacier sliding (e.g. Van de Wal et al., 2008; Sole et al., 2013) precludes us from applying a temporally evolving basal friction.

The model employs a crevasse-depth calving criterion based on crevasses opening by longitudinal acceleration towards the calving front. Calving occurs when surface crevasses penetrate the glacier thickness, or when surface and basal crevasses meet, whichever occurs first. Benn et al. (2007) and Nick et al. (2010) describe this criterion in detail. A calving parameter ('crevasse water depth') of 100 m is used for the spinup. This parameter is difficult to measure directly even for contemporary glaciers, but is necessary to calibrate the model when reproducing the Younger Dryas grounding line position at the Halsnøy moraine (Fig. 3a). Our value is comparable to what is used in a 1D-flowline model applied to synthetic outlet glaciers by Nick et al. (2010), 60% lower than what is used for Jakobshavn Isbræ during the cold Little Ice Age (1-D flowline model; Steiger et al., 2018), but roughly twice that used for a range of present-day western Greenland glaciers (2-D planview model; Choi et al., 2018). Note however that the crevasse water depth used in the flowline model is likely exaggerated, since it also implicitly accounts for the neglected frontal ice shelf melt (Steiger et al., 2018; see Section 3.3).

The calving law we use is physically-based and provides a link between near-front flow through longitudinal acceleration and mean rates of calving (Benn et al., 2007; Nick et al., 2010). This is likely an important mechanism that contributes to calving in a given setting (Joughin et al., 2008; Walter et al., 2010), but may be less appropriate for undercut glaciers where frontal melt influences calving (O'Leary and Christoffersen, 2013; Rignot et al., 2015; Benn et al., 2017). However, the depth-integrated nature of the flowline model does not allow for depth-variable submarine melt rates (see Section 3.3).

Runs are performed on an initial spatially uniform horizontal grid resolution of 500 m and we track the grounding line based on a flotation criterion (Van der Veen and Whillans, 1996). Because the grid tracks grounding line migration and the number of grid points are constant throughout a simulation, the grid gets compressed accordingly as the grounding line retreats up the fjord. The model grid resolution thus increases to ~350 m as retreat progresses towards the fjord head at Eidfjord. We assume no ice influx at the ice divide at the upper model boundary, implying a velocity $U(x = 0) = 0$.

3.3. Glacier width calculation

Ice flux is calculated according to the varying cross-sectional topography. At each time step and for each grid point, the width at the surface is calculated by finding the intersection between the ice surface and the lateral topography. This intersection, or trimline, is thus determined by the slope in the corresponding zone (Fig. 2c). Therefore, the model glacier width varies with time as ice thickness varies, as in the real-world case, intersecting the fjord walls ('trimlines') at different elevations at different times. At each model time step, ice flux is corrected according to the sloping fjord walls within each zone covered by the glacier.

We do not allow ice discharge between Hardangerfjorden's main trunk and the fjord arm Sørfjorden (at km 65–70 in Fig. 2a). This assumption is justified by reconstructed ice flow directions based on glacial striae suggesting no significant 'ice leakage' into Sørfjorden (Holtedahl, 1975; Hamborg and Mangerud, 1981).

3.4. Surface mass balance and ocean forcing

The surface mass balance (SMB) rate at a certain elevation z is given by

$$\dot{B}(z) = \Gamma(z - z_{ELA}) \tag{2}$$

where $\Gamma = \partial\dot{B}/\partial z$ is the vertical mass balance gradient and z_{ELA} represents the equilibrium line altitude (ELA). A gradient $\Gamma = 0.005$ is used, which is similar to observations from Greenland, Alaska, and Norway (Van de Wal et al., 2005; Rea and Evans, 2007; Van Beusekom et al., 2010; Huss and Farinotti, 2012). For simplicity, the surface mass balance forcing is kept constant throughout the simulations, meaning we exclude the surface mass balance-elevation feedback, as in similar studies (Nick et al., 2013; Bassis et al., 2017). However, we test the importance of this feedback in Section 5.4.

As ocean forcing, we apply spatially uniform submarine melt rates at the floating ice base from the grounding line to the terminus, while horizontal melt at the calving face is not included. As the model is 1-D depth-integrated, it is not numerically possible to apply any horizontal melt (see further discussion in Section 6.2).

4. Experimental setup

4.1. Simulating the Younger Dryas glacier

The model is spun up to steady-state for 1000 model years with a constant climate, using the uplift-corrected YD ELA. At the end of the spin-up, the grounding line and calving front positions change by less than 0.5 m a^{-1} and the total ice volume changes by ~0.01 km^3 a^{-1}. We assume a submarine melt rate of 10 m a^{-1} (Bakke et al., 2009; Dokken et al., 2015), close to modern annual melt rates for outlet glaciers in northern Greenland (e.g. Rignot and Steffen,

2008).

The simulated YD grounding line and surface topography (Fig. 3b) agree well with reconstructions by Mangerud et al. (2013) (Fig. 3a), except for a ~100–300 m too thick glacier in the interior and a ~100–300 m thinner glacier towards the front, where the latter may be related to uncertainties in our choice of model parameters, or the surface mass balance parameterization. Note however, that Mangerud's et al. (2013) reconstruction in the interior was merely an extrapolation assuming plastic ice flow (Nye, 1951, 1952, 1953), and should therefore be considered a crude estimate rather than a tight model constraint.

4.2. Younger Dryas to Holocene retreat

Mangerud et al. (2016) found that the ELA in the middle part of Hardangerfjorden was 880 m a.s.l. during the YD, which is 460 m lower than today. Based on the documented rapid climatic changes at the YD–Holocene boundary (Section 2.2), we raise the ELA by a 350 m step from 880 to 1230 m a.s.l. at 11.6 ka BP, consistent with the early Holocene climate being slightly cooler than the present (Eldevik et al., 2014). Sensitivity experiments with a gradual instead of a step increase in the forcing, suggest that this instant forcing perturbation plays a minor role for our results (see Sect. 5.4).

Alongside atmospheric changes, we increase submarine melt rates from 10 to 20 m a $^{-1}$. This estimate is based on (i) a 3–5 °C warming of sea surface temperatures (SSTs) in the Norwegian Sea at the YD-Holocene transition (Bakke et al., 2009; Eldevik et al., 2014; Dokken et al., 2015); and (ii) an estimated 80–140% increase in submarine melt in response to a similar warming of fjord waters in Greenland observed over recent decades and projected for the year 2100 (Slater et al., 2016; Hanna et al., 2011; Fettweis et al., 2013). The warm-water mollusc *Mytilus edulis* has been found in glacimarine sediments in the mid-fjord area near Tørvikbygd (Romundset et al., 2010), located on the opposite side of the fjord from Jondal (cf. Figs. 2a and 3a). *Mytilus edulis* is a shallow-water mollusc that requires summer sea temperatures of 4–6 °C, and in northwestern Europe and into the Arctic it is closely linked to warm Atlantic Water (Mangerud and Svendsen, 2018). During the Bølling-Allerød period it is present in western Norway, but disappears during the Younger Dryas. During the Holocene Thermal Maximum it is common on Svalbard, but becomes extinct 3700 years ago and re-immigrates in 2004 due to the recent climate warming (Mangerud and Svendsen, 2018). The finding of *Mytilus edulis* in Hardangerfjorden's mid-fjord area, dated to about 11.4 ka BP (Romundset et al., 2010), suggests that warming Atlantic Water (Eldevik et al., 2014) entered the fjord during the deglaciation, following the YD-Holocene transition.

An ensemble of simulations, using different ELAs and submarine melt rates, explores how sensitive the modelled retreat rates (Fig. 12a) and duration (Fig. 12b) are to the climate and ocean forcing imposed. This is assessed in detail in Section 5.4.

The calving parameter ('crevasse-water depth') is the least constrained parameter, yet it influences calving rates and determines the cliff height for a floating ice shelf (Schoof et al., 2017). We therefore run the model with different step parameter changes seeking to find values that capture the 500-year retreat from Halsnøy to Eidfjord within dating uncertainties (±100 years). Given the aforementioned changes to the ELA (+350 m) and submarine melt rate (+100%) we found that crevasse water depths increasing within a range of 0–75% capture retreat within dating uncertainties (see Section 5.4). For the main 500-year retreat scenario ('best-guess') detailed in Figs. 3–5, we choose the simulation with a 20% increase of the crevasse water depth (+20 m).

4.3. Sensitivity to climate forcing and iceberg calving

To test the robustness of our results and the relative importance of the different forcing factors, we performed simulations with ELA changes ranging from +280 to +500 m, reflecting uncertainty in the underlying reconstructions. We also investigated the effect of including the surface mass balance-elevation feedback (e.g. Harrison et al., 2001). In addition, we tested an ensemble of submarine melt rates, from keeping it constant (10 m a^{-1}) throughout the 11.6 to 11.1 ka BP-period, to a four-fold increase (40 m a^{-1}), which is at the high-end expected for Greenland outlet glaciers in the future. For the calving parameter, we performed experiments ranging from constant to a 75% increase, reflecting ranges used for Greenland outlet glaciers (Nick et al., 2013; Steiger et al., 2018).

5. Results

5.1. An episodic 500-year retreat

Our model simulations suggest a rapid and highly variable grounding line retreat from the Halsnøy YD moraine at the fjord mouth (11.6 ka BP) to the Eidfjord early Holocene moraine at the fjord head (11.1 ka BP; Figs. 3–5). Retreat rates vary from 50 to 2500 m a^{-1}, with a mean of 272 m a^{-1} (Fig. 5b), comparable to the mean retreat rate of 240 ± 70 m a^{-1} estimated from the reconstructions by Mangerud et al. (2013).

Following the retreat from Halsnøy, a 15 km long ice shelf gradually develops (Figs. 3b and 5d). Buttressing by the ice shelf increases accordingly (Fig. 5e). However, the ice shelf length decreases as the glacier retreats towards the sill at Jondal, with a minimum of 5 km floating ice remaining at c. 11.3 ka BP. As a result, lateral drag provided by the shelf drops by 75% (Fig. 5e), accompanied by a velocity speedup at the grounding line by ~40% (Fig. 3d). As the grounding line retreats along the shoaling bed to Jondal, (c. km 115–110, Fig. 3b), the velocity at the grounding line (Fig. 3d) increases further. This speedup is consistent with mass conservation, since the smaller cross-sectional area at the Jondal sill requires a higher velocity to maintain the same flux.

Once the grounding line dislodges from the mid-fjord sill at Jondal, the grounding line retreats rapidly down the retrograde slope, with a retreat of ~30 km in 60 years (Fig. 3b and c). This gives an average retreat rate of 500 m a−1, with an ephemeral maximum of 5 km retreat within one year (Fig. 5b). This retreat is accompanied by an extension of the ice shelf length to 20 km, deceleration of the calving front velocity by ~50% and a simultaneous velocity slowdown by ~60% at the grounding line (Fig. 3d), as it retreats along the retrograde bed from km 110 to 90 (Fig. 3b). Note the difference here between ice velocity at the grounding line (which decreases; Fig. 3d), and the retreat rate of the grounding line (which increases; Fig. 5b). As given by mass conservation, the deeper grounding line requires slower velocities to maintain the same flux. The grounding line flux increases prior to this unstable retreat, and gradually decreases as retreat progresses into the over-deepened basin upstream of the Jondal sill (Figs. 3e and 5c).

In contrast to the behavior of the grounding line, the retreat of the calving front and the surface thinning is close to linear throughout the simulation (Figs. 3b and 5a), with decadal-scale periods of accelerated retreat out-of-phase with the grounding line retreat (Fig. 5b). The associated calving flux varies by up to ~100% around a mean rate of ~1.5 km^3 a−1 (0.04 mSv) over the course of the retreat. The total volume lost from fjord mouth to fjord head is 1387 Gt, or 3.84 mm sea-level equivalent. For extended periods, the grounding line flux is larger than the concurrent calving rates (Fig. 5c and d), resulting in ice shelf extension (Figs. 3b and 5d).

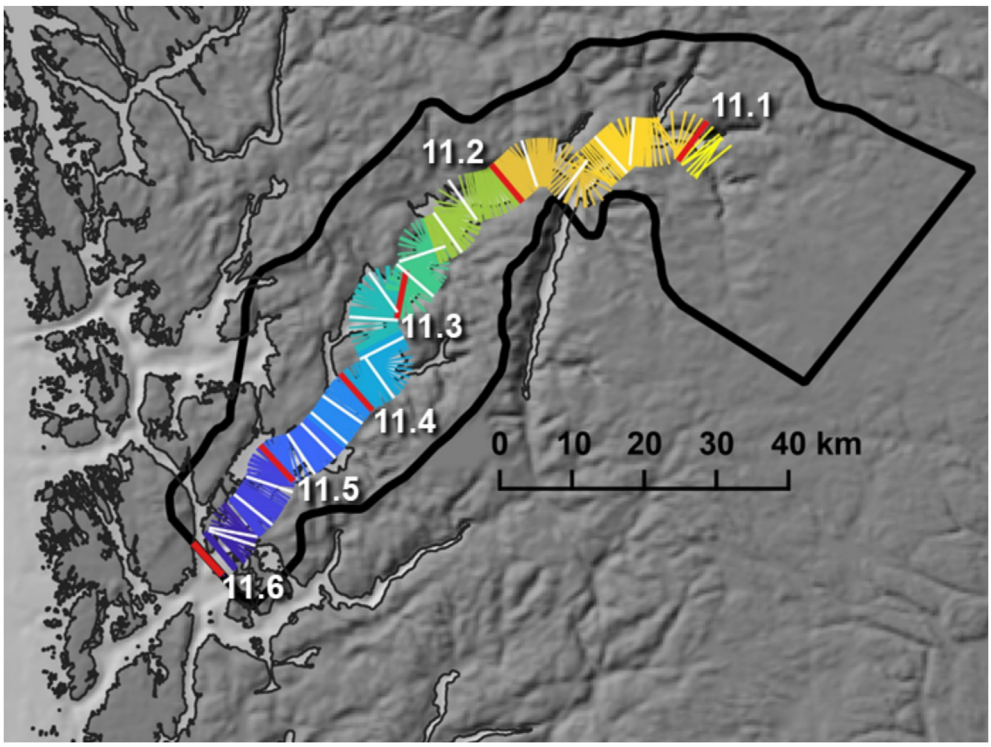

Fig. 4. Simulated yearly front positions of Hardangerfjorden glacier from the dated Younger Dryas moraine at the fjord mouth at Halsnøy to the dated moraine at the fjord head in Eidfjord. 20-year positions are highlighted in white, with ages given as thousand years before present. Time coloring as in Fig. 3.

Frontal and grounding line retreat rates vary out-of-phase (Fig. 5a and b) primarily due to bathymetric controls and ice shelf growth and collapse (Fig. 5d), as further detailed in Section 5.3 below. A similar retreat pattern is present regardless of the climate forcing (Fig. 6).

5.2. Dominance of surface mass balance on centennial timescales

The retreat from Halsnøy is dated to have started 11.6 ± 0.1 ka BP, reaching Eidfjord at 11.1 ± 0.1 ka BP. Within radiocarbon dating uncertainties, the retreat lasted 300–700 years, with a likely range of 400–600 years. The change in ELA at the YD–Holocene transition is not known precisely, and precipitation changes are poorly constrained, making direct translation between ELA and temperature and precipitation changes challenging. Here, we are interested in the range in ELA, submarine melt rates and calving parameter capable of triggering and driving the documented rapid retreat.

The simulation that reproduces the 500-year retreat, and is most consistent with the reconstructed climate and ELA (see Sect. 2.2 and 4.3), is hereafter termed the 'best-guess'. Note, however, that several experiments within our ensemble are able to reproduce retreat within dating uncertainties, rendering a retreat duration of 500 ± 100 years (Figs. 6 and 7b). This implies that the best-guess simulation carries the parameters that best match the reconstructed retreat. Nevertheless, the best-guess parameters are not necessarily physically representative of the true ELA, submarine melt rates, and calving at the YD-Holocene transition. For example, we have excluded the surface mass balance–elevation feedback in most simulations (see end of this section) and our implementation of submarine melt is simple (Section 3.3), and thus the 'real' ELAs and submarine melt rates may have been different from what is imposed here.

In the best-guess simulation, we change the surface mass balance, the submarine melt and the calving parameter simultaneously. Based on additional sensitivity experiments (Sect. 5.3) we find that changing the surface mass balance is the most efficient driver of the retreat (Fig. 7b), but also that changes to the ocean forcing shortens the duration of the retreat by 100–150 years, within the expected submarine melt rates (15–40 m a^{-1}). The calving parameter has less impact; only shortening the retreat by 40 years within a plausible parameter range (+50% increase in crevasse water depth), a timescale which is still within the dating uncertainties.

The effect of the surface mass balance–elevation feedback is striking, but is excluded in most simulations, also for the 'best-guess' experiment. Including this feedback in our 'best-guess' YD to Holocene scenario (+350 m ELA, +20% calving parameter, +100% submarine melt rates), the retreat from fjord mouth to fjord head is reduced from 500 to 245 years (experiment 'best-guess-fb' in Table 1). Even without a change in calving and submarine melt rates, the surface mass balance-elevation feedback strongly amplifies surface thinning, and the retreat is completed in 280 years (experiment ela1230wd100subm10-fb in Table 1), suggesting an underestimation of the role of the atmospheric forcing compared to the ocean.

5.3. Episodic retreat set by fjord bathymetry

Our simulations suggest that the long-term retreat of the Hardangerfjorden glacier was driven by atmosphere and ocean warming, whereas the highly episodic retreat was paced by the fjord bathymetry (Figs. 3 and 4). Our ensemble of simulations allows us to assess what factor(s) govern the simulated retreat. We find that the fastest retreat, exceeding 400 m a^{-1}, occurs predominantly on retrograde slopes (e.g. along the overdeepening upstream of the Jondal sill), while retreat is significantly slower over prograde slopes (Fig. 8). Interestingly, retreat rates stay below the mean modelled retreat rate of 272 m a^{-1} during most of the retreat

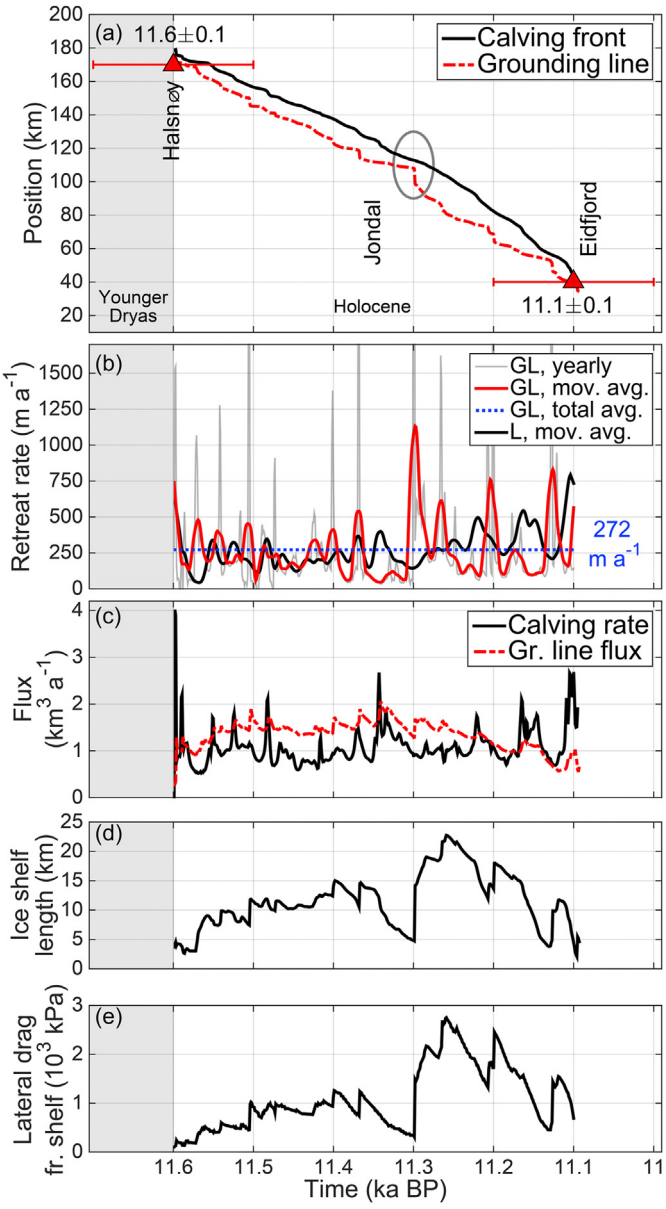

Fig. 5. Simulated evolution of Hardangerfjorden glacier from the dated Younger Dryas moraine at the fjord mouth at Halsnøy to the dated moraine at the fjord head in Eidfjord. (a) Calving front and grounding line position, (b) frontal (L) and grounding line (GL) retreat rate, and its moving (20-year) and total (500-year) average (yearly frontal retreat rates are not shown for visibility), (c) calving rate and grounding line flux, (d) ice shelf length, and (e) integrated lateral drag from floating ice, calculated as $\tau_{lat,\,shelf} = \int_{x_g}^{x_c} \tau_{lat}\,dx$, where x_g and x_c is the grounding line and calving front positions, respectively.

from Halsnøy to Eidfjord (Fig. 5b), punctuated by short-lived phases of accelerated retreat on mainly neutral to retrograde slopes (cf. Figs. 3b and 5b).

In contrast to bedrock slopes, grounding line retreat rates are largely independent of water depth (Fig. 9), ice shelf length (Fig. 10) and velocity at the grounding line (Fig. 11). Based on Fig. 9, there is an apparent threshold of water depths of c. 400 m, above which simulated grounding line retreat rates are found to be greater than the mean reconstructed rates of 240 m a^{-1} (Mangerud et al., 2013). However, there are some exceptions where the retreat rates exceed 1000 m a^{-1} and even 2000 m a^{-1} at depths shallower than 400 m (Fig. 9).

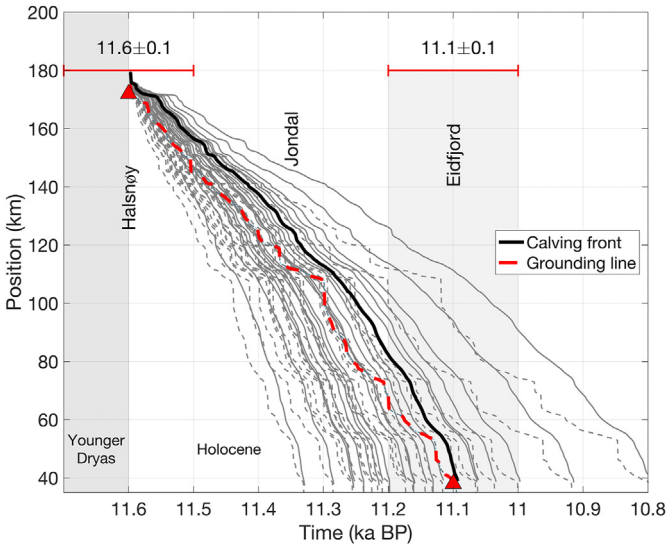

Fig. 6. Simulated evolution of the calving front (solid lines) and grounding line (dashed lines) from the dated Younger Dryas moraine at the fjord mouth at Halsnøy to the dated moraine at the fjord head in Eidfjord, showing an ensemble of experiments with different atmospheric (ELA) and oceanic (submarine melt rate) forcing. All experiments use a 20% increase in the crevasse water depth, cf. Table 1.

Neither the ensemble, nor the best-guess simulation show clear patterns regarding how ice shelf length affects grounding line retreat rates (Fig. 10). Fast retreat exceeding 1000 m a^{-1} can occur both with long and short ice shelves, though there is a slight tendency towards shorter shelf lengths and faster retreat. A similar pattern can be seen for the velocity at the grounding line and the retreat rates: no clear relationship can be found, and if anything, there is a tendency towards slow velocities at the grounding line concurrent with fast retreat (Fig. 11).

Throughout the retreat, we find that deeper water facilitates longer ice shelves (Fig. 12), yet as we have seen, neither water depth (Fig. 9), nor ice shelf length (Fig. 10) correlates with grounding line retreat. Our results suggest a persistent ice shelf during retreat: 5 km long when the glacier is grounded on the sills at Halsnøy and Jondal, growing to a length of 20–25 km at over-deepened sections of the bed (Figs. 3b and 5d).

The modelled intermittent slowdown of the retreat close to Jondal (at ~km 110 in Figs. 3 and 5a) is supported by small ice marginal deposits at the northern flank of the fjord, indicating a brief period of grounding line stability at this location (Aarseth, 2004). Based on the model results, we estimate the temporary stillstand to have occurred at 11.3 ka BP. This is consistent with the minimum age of 11.3 ka BP at this location postulated by Romundset et al. (2010), based on terrestrial plant remains and mollusk shells in sediment cores from several bogs and lakes along the northern brink of the fjord. While we have tuned the model parameters to simulate the duration of the retreat from the fjord mouth to the fjord head, it is encouraging that the unconstrained transient modelled retreat agrees with the mid-fjord observations at Jondal.

5.4. Sensitivity to climate forcing and iceberg calving

A gradual increase in forcing (ELA, submarine melt, and crevasse water depth) is likely more realistic than our imposed instant changes. However, sensitivity tests reveal that our step perturbations shorten retreat by only 15 years at Eidfjord compared to a linearly increasing forcing over 100-years (experiment *best-guess-*

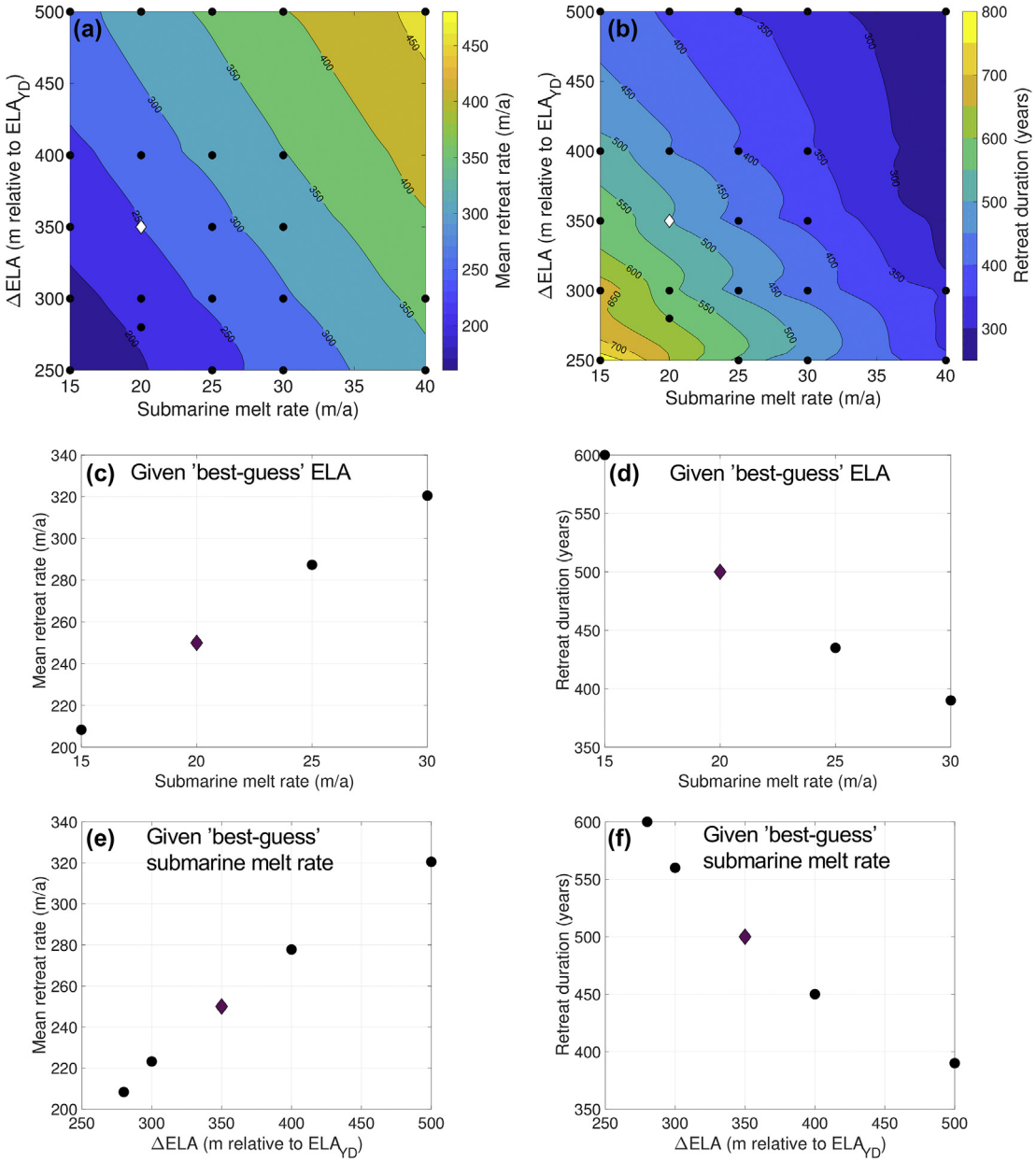

Fig. 7. (a) Mean modelled retreat rates and (b) retreat duration from the fjord mouth to the fjord head in response to changes in the ELA and submarine melt rates, with the Younger Dryas glacier and climate (ELA = 880 m a.s.l., submarine melt rate = 10 m a^{-1}) as initial conditions. Individual experiments (black dots) and best-guess experiments (white diamond) are highlighted. Shown is also (c) mean retreat rates, given the best-guess change in ELA (+350 m, to 1230 m a.s.l.), (d) retreat duration, given the best-guess change in ELA, (e) mean retreat rates given the best-guess submarine melt rate (20 m a^{-1}), and (f) retreat duration given the best-guess submarine melt rate. Best-guess experiments in (c)–(f) are highlighted with purple diamonds. All experiments shown use a 20% increase in the crevasse water depth, cf. Table 1. (For interpretation of the references to color in this figure legend, the reader is referred to the Web version of this article.)

linear in Table 1). The step forcing causes the grounding line to retreat past a given location 5–15 years earlier than with the gradually increasing forcing. Our results thus show negligible dependence to how the forcing is applied at the YD–Holocene transition.

Raising the ELA by 500 m (880–1380 m a.s.l.) instead of the 'best-guess' 350 m gives a retreat from Halsnøy to Eidfjord in 520 years, without accounting for changes in the crevasse water depth or ocean forcing (experiment *ela1380wd100subm10*). Since this is close to the reconstructed duration of retreat, and we expect large changes in the ocean forcing based on offshore marine records (Bakke et al., 2009; Dokken et al., 2015) as well as local glacio-marine empirical evidence mid-fjord from the period (Romundset et al., 2010), this ELA increase is likely too strong. A more feasible scenario, in light of the proxy records, is our 'best-guess' YD-to-Holocene scenario, which includes a 350 m increase in ELA, a doubling of submarine melt rates, and a 20% increase in the calving parameter relative to YD conditions (*best-guess* in Table 1).

Alternatively, assuming the ELA rose by only 300 m, keeping the same calving parameter and melt rates as in the best-guess scenario, the retreat takes 60 years longer (560 years; experiment *ela1180wd120subm20* in Table 1). An additional 25% increase in melt rates (25 m a^{-1}) is required to compensate for the 50 m smaller ELA increase (485 years; experiment *ela1180wd120subm25* in Table 1).

Given our 'best-guess' doubled submarine melt rates and 20%

Table 1
Forcing and parameter values for the YD glacier (spin-up), Halsnøy-to-Eidfjord modelled 500-yr retreat ('best-guess'), and sensitivity experiments. Listed are equilibrium line altitudes (ELA), crevasse water depths (wd), submarine melt rates (M_b), whether a surface mass balance (SMB)-elevation feedback (fb) is included, and the modelled duration of retreat from the Younger Dryas moraine at Halsnøy to the early Holocene Eidfjord moraine 125 km upstream. The retreat lasted 500 ± 100 years according to the dated moraines at the fjord mouth and fjord head. The forcing (ELA, wd and M_b) for the best-guess-linear experiment increases linearly for 100 years, and are constant thereafter, while for all other retreat experiments, an instant step-change in the forcing parameters is imposed. The ensemble of simulations in this table is visualized in Fig. 6 (evolution of the calving front and grounding line retreat) and Figure 7 (retreat rates and duration with respect to ELA and submarine melt rates).

Experiment	ELA (m a.s.l)	wd (m)	$\dot{M}_b$ (m a^{-1})	SMB-elev. feedback (y/n)	Retreat duration (yrs)
YD glacier (spinup)	880	100	10	no	–
ela1130wd120subm15	1130	120	15	no	800
ela1130wd120subm25	1130	120	25	no	535
ela1130wd120subm30	1130	120	30	no	465
ela1130wd120subm40	1130	120	40	no	375
ela1160wd120subm20	1160	120	20	no	600
ela1180wd120subm15	1180	120	15	no	685
ela1180wd120subm20	1180	120	20	no	560
ela1180wd120subm25	1180	120	25	no	485
ela1180wd120subm30	1180	120	30	no	425
ela1180wd120subm40	1180	120	40	no	345
ela1230wd100subm10-fb	1230	100	10	yes	280
ela1230wd120subm15	1230	120	15	no	600
ela1230wd100subm20	1230	100	20	no	530
ela1230wd100subm25	1230	120	25	no	435
ela1230wd100subm30	1230	120	30	no	390
best-guess	1230	120	20	no	500
best-guess-linear	1230	120	20	no	515
best-guess-fb	1230	120	20	yes	245
ela1230wd120subm30	1230	120	30	no	390
ela1230wd150subm20	1230	150	20	no	460
ela1230wd175subm20	1230	175	20	no	410
ela1280wd120subm15	1280	120	15	no	535
ela1280wd120subm20	1280	120	20	no	450
ela1280wd120subm25	1280	120	25	no	400
ela1280wd120subm30	1280	120	30	no	360
ela1380wd100subm10	1380	100	10	no	520
ela1380wd100subm15	1380	120	15	no	440
ela1380wd100subm20	1380	100	20	no	400
ela1380wd120subm20	1380	120	20	no	390
ela1380wd120subm25	1380	120	25	no	345
ela1380wd120subm30	1380	120	30	no	315
ela1380wd120subm40	1380	120	40	no	270

higher crevasse water depth, an ELA increase of anything from 280 to 500 m is possible based on dating uncertainties (Fig. 7f). Analogously, assuming the 'best-guess' ELA increase of +350 m and 20% higher crevasse water depth, melt rates between 15 and 30 m a^{-1} (50–200% increase relative to YD) can drive retreat to Eidfjord consistent with the radiocarbon dated age of 11.1 ± 0.1 ka BP (Fig. 7d).

For the *best-guess* experiment, the crevasse water depth is increased from 100 to 120 m, rendering a retreat in 500 years (Section 5.1). If we instead keep the crevasse water depth unchanged (0% increase), retreat duration increases to 560 years (experiment *ela1230wd100subm20* in Table 1). Conversely, if we increase the crevasse water depth to 175 m (75% increase), retreat duration is shortened to 410 years (experiment *ela1230wd175-subm20* in Table 1). In other words, assuming the 'best-guess' changes to the ELA and the submarine melt rates, the crevasse water depth can be between 100 and 175 m in order to reproduce the retreat within dating uncertainties.

We can estimate how much an increase of the ELA and submarine melt rate shorten the retreat from Halsnøy to Eidfjord (given our 20% higher crevasse water depth). For every 10 m ELA increase, the duration of the retreat decreases by 7–20 years (Fig. 7b and Table 1). Similarly, for every 1 m a^{-1} increase in the submarine melt rate, the retreat duration is shortened by 9–12 years. The impact of these atmosphere and ocean changes is not linear with respect to retreat duration. For more extreme changes in forcing, the relative change in duration is less pronounced than for moderate changes (Fig. 7b). For example, the retreat duration is shortened by 60 years by increasing the ELA by 350 instead of 300 m (Fig. 7f). When ELA changes become larger, the impact on retreat duration is smaller; for example, shortening the retreat by 60 years requires an ELA increase from 400 to 500 m in the high end of the ensemble. A similar pattern can be found with respect to submarine melt rates (Fig. 7d).

6. Discussion

6.1. Surface-melt driven retreat paced by bathymetry

We find that the rate of grounding line retreat is largely independent of the water depth at the grounding line (Fig. 9). This runs counter to what has been suggested for some calving glaciers in Alaska, western Greenland and Patagonia (Pelto and Warren, 1991; Hanson and Hooke, 2000), but is consistent with a theoretical analysis and numerical model experiments by Schoof et al. (2017). The latter concluded that for glaciers with floating tongues, the calving cliff height is independent of water depth and instead proportional to the crevasse water depth imposed. Nonetheless, based on Fig. 9, there is an apparent threshold of water depths of c. 400 m, above which most of the retreat rates are greater than the mean rates of 240 m a^{-1} reconstructed by Mangerud et al. (2013). However, retreat rates exceeding 1000 m a^{-1} and even 2000 m a^{-1} at depths shallower than 400 m are also possible (Fig. 9).

As detailed in Section 5.3, ice-shelf length varies drastically throughout the retreat (Fig. 5d). The model includes lateral drag acting on the shelf, and any buttressing along the shelf gets

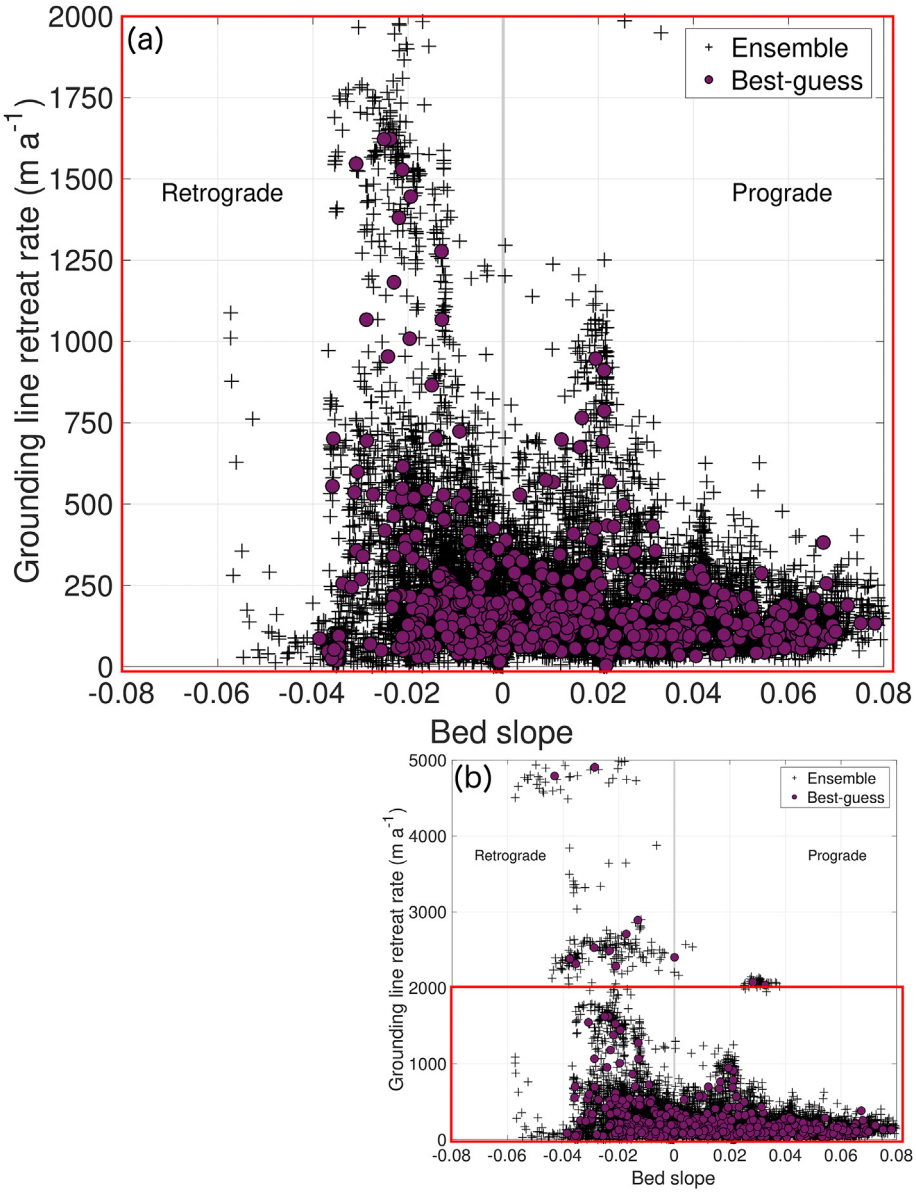

Fig. 8. Grounding line retreat rates are controlled by bedrock slope $\frac{\partial z_b}{\partial x}$ around the grounding line. Here, zb is the bedrock elevation and x is the horizontal distance. Bed slopes are measured using central differencing around the nearest grid points, averaging bed slopes over 700–1000 m around the grounding line. Positive slopes imply a prograde bed (sloping towards the sea), negative means a retrograde bed (deepening inland). In (a) retreat rates up to 2000 m a^{-1} are shown in greater detail, corresponding to the red square in (b). (For interpretation of the references to color in this figure legend, the reader is referred to the Web version of this article.)

transmitted to upstream grounded ice. We should thus expect some upstream effects associated with ice-shelf length variations. While some concurrent upstream velocity variations occur (Fig. 3d), our findings suggest that ice shelf variations appear to be the *result* rather than the *cause* of changing grounding line retreat rates. In particular, modelled ice-shelf lengths correlate with the water depth at the grounding line (Fig. 12), yet both of these are *associated with* rather than the *cause of* fast grounding line retreat of Hardangerfjorden glacier, as detailed in Section 5.3.

Instead, our assessment of the controls of the retreat in our ensemble and best-guess simulations (Section 5.3) show that the simulated grounding line retreat is mainly governed by local bedrock slopes (Fig. 8). In contrast to water depth (Fig. 9) and ice shelf length (Fig. 10), we find a relationship, albeit weak, between the bedrock slope and the retreat rate of the grounding line (Fig. 8). The latter finding is in line with theory (e.g. Weertman, 1974; Schoof, 2007), but our simulations suggest that the relationship between topography and retreat is not straightforward and cannot be used uncritically to estimate retreat rates.

We find a high sensitivity to the surface mass balance (Sect. 5.2), here parameterized using the ELA and a vertical mass balance gradient Γ (Sect. 3.3). Better constraints on the ELA and its underlying parameters (vertical mass balance gradient, temperature and precipitation) should be prioritized in future work, through developing parameterizations and improving understanding of the underlying ice–atmosphere interactions and their influence on the surface mass balance. Moreover, our finding that the surface mass balance–feedback strongly accelerates retreat over multi-centennial time scales is relevant for future projections. This feedback is usually not included in future projections for the next century, but our results suggest that projections beyond 2100 may underestimate retreat if this feedback is left out.

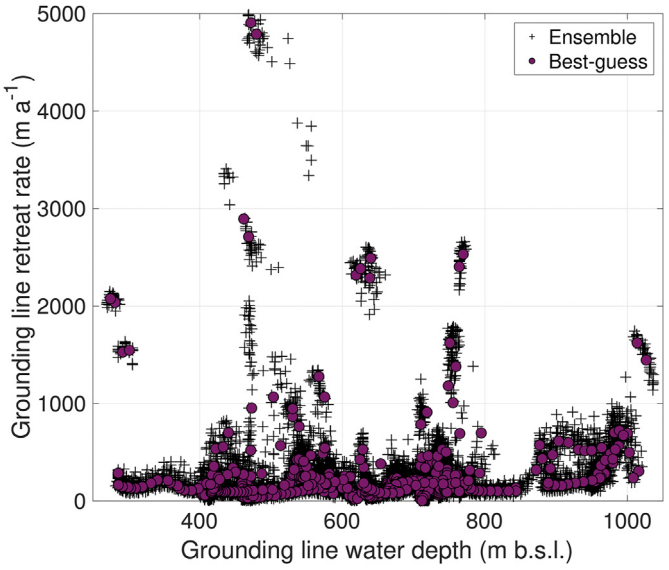

Fig. 9. Grounding line retreat rates vary largely independent of water depth at the grounding line. Ensemble (black crosses) and best-guess experiments (purple dots) are shown. (For interpretation of the references to color in this figure legend, the reader is referred to the Web version of this article.)

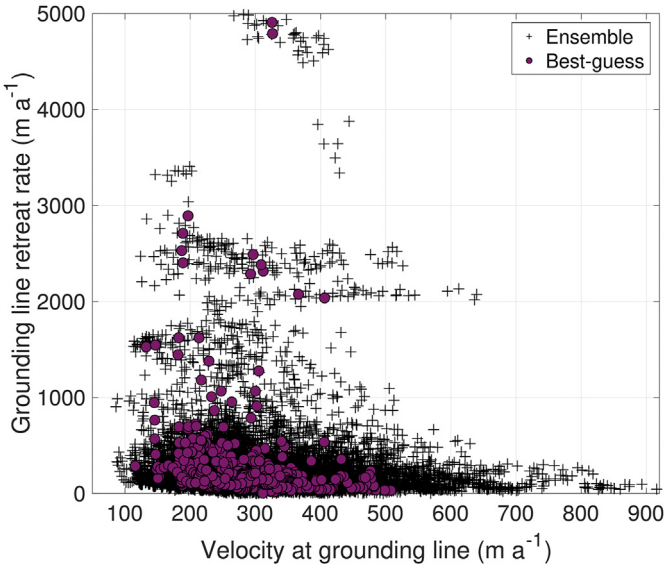

Fig. 11. No apparent relationship is found between grounding line retreat rates and ice velocity at the grounding line. Ensemble (black crosses) and best-guess experiments (purple dots) are shown. (For interpretation of the references to color in this figure legend, the reader is referred to the Web version of this article.)

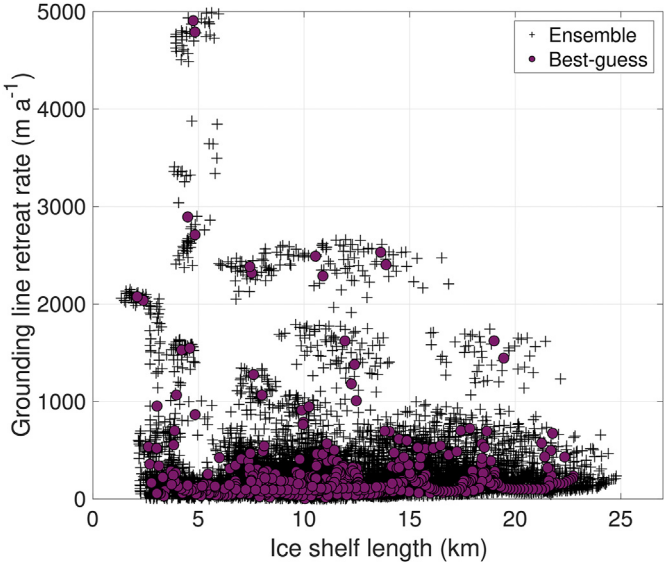

Fig. 10. Grounding line retreat rates are largely independent of ice shelf length in our modelled experiments. Ensemble (black crosses) and best-guess experiments (purple dots) are shown. (For interpretation of the references to color in this figure legend, the reader is referred to the Web version of this article.)

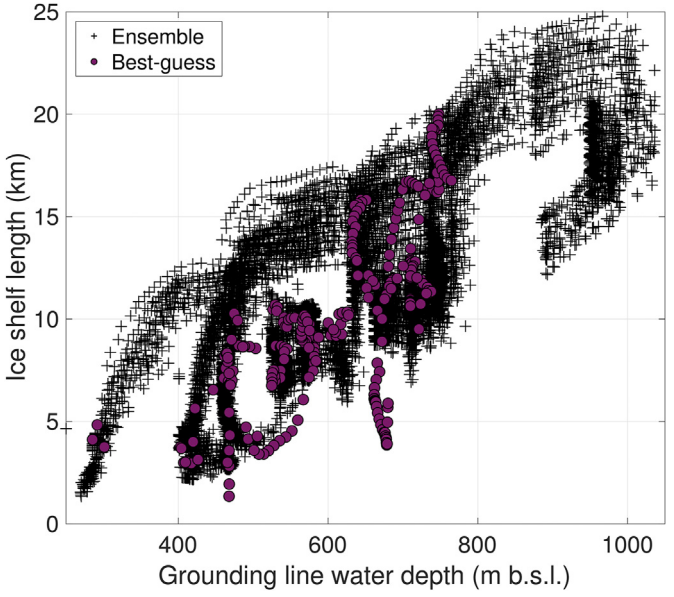

Fig. 12. Ice shelf length during the retreat increases with water depth at the grounding line. However, neither ice shelf length nor water depth control grounding line retreat rates (Figs. 8 and 9). Ensemble (black crosses) and best-guess experiments (purple dots) are shown. (For interpretation of the references to color in this figure legend, the reader is referred to the Web version of this article.)

6.2. Limits to ocean melt and calving dynamics

As described in Section 3.4, it is not possible to include horizontal frontal melt in a depth-integrated flowline model. Alternatively, the tuned calving parameter ('crevasse water depth') may be interpreted as partly accounting for the neglected ice shelf frontal melt (Steiger et al., 2018). Some flowline model studies (e.g. Bassis et al., 2017) have added "artificial" melt a few grid points upstream of the terminus, to mimic the effect of frontal melt. We tested this approach during the spin-up phase, aiming to trigger frontal retreat off the Halsnøy sill by the ocean forcing alone. We found, however, that adding additional melt two grid points (~1 km) upstream of the front was not enough to trigger retreat; an additional ELA increase is needed. Moreover, because we apply uniform vertical melt along the entire ice shelf base, the effect of horizontal frontal melt may be accounted for implicitly. In reality, melt at an ice shelf base decreases gradually towards the ice shelf front (that is, towards the surface water layer, see e.g. Jenkins, 2011). This means that our uniformly imposed ocean forcing potentially overestimates ice shelf basal melt close to the ice shelf front. Since we neglect (thereby underestimate) ice shelf frontal melt, the two effects are likely to partly cancel.

The impact on the model glacier by excluding frontal melt likely varies throughout the retreat, as the ice shelf area varies. For example, when the ice shelf is long (e.g. upstream of the Jondal sill) the effective area available for frontal melt is small compared to the area of the ice shelf draft (Figs. 3b and 5d). In contrast, when the ice shelf is short (e.g. at the YD position at the Halsnøy sill, and at the Jondal sill), frontal ice shelf melt may be more important, leading us to potentially underestimate the rate of retreat.

Recent work has shown that grounding line dynamics may be dependent on the calving law chosen (Schoof et al., 2017; Haseloff and Sergienko, 2018), though these studies have neglected the effect of submarine melt. Since calving dynamics is an area of intense research (Bassis and Walker, 2012; Pollard et al., 2015; Benn et al., 2017), testing the impact of different calving laws remains a priority for future studies in similar settings.

6.3. Hardangerfjorden glacier as an analogue for Jakobshavn Isbræ

The Hardangerfjorden glacier and its retreat history is an analogue to the retreat history of Jakobshavn Isbræ and other similar outlet glaciers in Greenland. The recent observed retreat of Jakobshavn Isbræ has gained considerable attention by the scientific community (e.g. Holland et al., 2008; Khazendar et al., 2019), as the marine outlet glacier has the potential to drain large amounts of ice from the Greenland Ice Sheet, thus contributing to an accelerated rise in sea level. However, the detailed observational record of Jakobshavn Isbræ is only a few decades long. Given the ability of marine outlet glaciers to integrate short-term variability in atmospheric and oceanic forcing, century-scale, kilometer-scale fluctuations in glacier extent are expected, even in a constant climate (Roe and O'Neal, 2009). This makes it hard, if not impossible, to assess the long-term response of an outlet glacier, such as Jakobshavn, to the recent observed changes in ocean and atmospheric climate.

Therefore, historical examples and long-term records are critical to assess the retreat dynamics of glaciers, including the marine outlet glaciers in Greenland. Hardangerfjorden offers such an example, with its highly resolved glacial topography and well dated retreat history starting at Halsnøy and ending at Eidfjord. This is perhaps the closest known analogue to the fjord of Jakobshavn. Jakobshavn Isbræ is known to have retreated from its Last Glacial Maximum extent to its Holocene minimum at 6–5 ka BP, before readvancing to a maximum in the Little Ice Age (Kajanto et al., 2020). The retreat rate varied between 225 m a^{-1} to 900 m a^{-1} (Streuff et al., 2017), not unlike the simulated rates found here for Hardangerfjorden.

Currently, the grounding line of Jakobshavn Isbræ has retreated approximately 20 km from its Little Ice Age maximum and is located at a tipping point, constrained by the bedrock topography of the narrow fjord. Although the future fate of the glacier is unknown, it is expected that, once a further retreat is triggered, fjord bathymetry rather than climate variability will govern the retreat rate (Kajanto et al., 2020).

6.4. Future stability of marine outlet glaciers

We show that retreat rates vary greatly over the course of the 500-year 'collapse' of the Hardangerfjorden glacier. The modelled grounding line retreat rate generally remains below the mean modelled retreat rate of 272 m a^{-1}, disrupted by irregular short-lived periods of swift retreat at rates ten times faster (c. 1000–5000 m a^{-1}; Figs. 5 and 8). This modelled swift retreat is similar to recent short-term retreat of several outlet glaciers in Greenland (Howat and Eddy, 2011; Rosenau et al., 2013), such as Jakobshavn Isbræ (c. 1000 m a^{-1}) and Helheim Glacier (c. 400 m a^{-1}).

The multi-centennial mean retreat rate of 272 m a^{-1} is among the highest reported for marine outlet glaciers (Briner et al., 2009; Young et al., 2011; Hughes et al., 2012; Mangerud et al., 2013; Stokes et al., 2014). Equally important, our simulations suggest that bathymetry, rather than climate, maintains fast retreat once triggered, and therefore episodes of enhanced retreat rates can only be sustained for a few decades at a time (Fig. 5b). Given these findings and the topographic similarity between Hardangerfjorden and the fjords of Greenland, which currently host hundreds of marine outlet glaciers, we postulate that the observed recent rapid retreat of many Greenland outlet glaciers may not be sustainable for longer than a few decades. While continued retreat is expected to be driven by a warming climate, transient retreat rates will strongly depend on the upstream fjord topography.

If the current anthropogenic emissions are left unabated, we are heading for a similarly rapid and pronounced climate warming (e.g. AMAP, 2017) and glacier melt as occurred in Hardangerfjorden in western Norway at the last glacial termination. Mean global temperatures 2–3 °C higher than pre-industrial levels are projected for the year 2100 given successful mitigation scenarios, with 4–5 °C warming a possibility in the high-end emission scenarios (Stocker et al., 2013). More importantly, the Arctic has warmed twice as much as the global mean over the past 50 years (Christensen et al., 2013), with autumn and winter temperatures expected to increase by 4–5 °C by mid-century (AMAP, 2017). Further, Arctic outlet glaciers may see autumn and winter temperatures rising by 10 °C towards the end of this century, resulting in longer and stronger melt seasons. Such atmospheric changes are capable of lifting ice sheet snow-lines (the ELA) at rates similar to those at the YD–Holocene transition in western Norway.

We therefore expect future climate warming to drive extensive, yet highly variable, retreat of the world's marine outlet glaciers over the coming centuries, with maximum retreat rates comparable to those found for the Hardangerfjorden glacier during the YD–Holocene transition.

7. Conclusions

We have assessed the triggers, drivers and transient dynamics of the deglaciation of Hardangerfjorden at the last glacial termination by using a simple ice-flow model constrained by well-dated moraines. The model includes an idealized oceanic and atmospheric forcing based on reconstructions and excludes the surface mass balance-elevation feedback. Our results suggest that the initial glacier retreat was triggered by a rise of the ELA, and that the 125 km-retreat over 500 years was sustained by increased surface melt and warming fjord waters. The modelled grounding line retreat rate generally fluctuates below the mean retreat rate of 272 m a^{-1}, which is one of the highest multi-centennial retreat rates known for marine outlet glaciers. Modelled gradual retreat is disrupted by irregular periods lasting a few decades each, with retreat rates ten times higher (c. 1000–5000 m a^{-1}).

Our findings suggest that once the retreat of a marine outlet glacier is triggered, inland-sloping fjord bathymetry, rather than climate, maintains the fast retreat. This implies that periods of swift retreat can only be sustained for a few decades at a time.

The simulated historic retreat of Hardangerfjorden glacier sheds light on the current retreat of marine outlet glaciers in Greenland and beyond, such as Jakobshavn Isbræ, where the recent rapid retreat triggered by climate warming, is expected to be highly

modulated by the fjord bathymetry.

Declaration of competing interest

The authors declare that they have no known competing financial interests or personal relationships that could have appeared to influence the work reported in this paper.

Acknowledgements

The research leading to these results received funding from the Research Council of Norway (project no. 229788), as part of the project Eurasian Ice Sheet and Climate Interactions (EISCLIM). The research has also received funding from the European Research Council under the European Community's Seventh Framework Programme (FP7/2007–2013)/ERC grant agreement 610055 as part of the ice2ice project. FMN was funded by the ConocoPhillips Northern Area Program (CRIOS: Calving Rates and Impact on Sea Level). HÅ was also supported by the Research Coucil of Sweden, grant no. 2016-04021.

We are indebted to Eva Bjørseth, who helped with scientific illustrations, and Kristian Vasskog for assistance with the overview map. Finally we would like to thank the editor and the two anonymous reviewers, whose comments greatly improved the manuscript.

Appendix A. Supplementary data

Supplementary data to this article can be found online at https://doi.org/10.1016/j.quascirev.2020.106645.

Author contributions

JM came up with the idea of the project, which was initiated by JM and JIS. The conceptual groundwork was done by JM and JIS, together with FMN and RG. Topographic data compilation and fjord geometry parametrization was performed by RG with input from HÅ. FMN provided the ice flow model, with new improvements specific to this work implemented by FMN and HÅ. HÅ designed and carried out model experiments with significant input from FMN and KHN. Model results were analysed by HÅ with considerable input from all co-authors. HÅ wrote the manuscript with feedback from all co-authors. Figs. 1, 2 and 4 were made by RG, while the other figures were done by HÅ.

References

Aarseth, I., 2004. Vidde, Dal, Fjord. Natur historisk vegbok Hordaland, Bergen Museum– Nord, Bergen, pp. 60–66.
Aarseth, I., Austbø, P., Risnes, H., 1997. Seismic stratigraphy of Younger Dryas ice-marginal deposits in western Norwegian fjords. Nor. Geol. Tidsskr. 77, 65–85.
Åkesson, H., Nisancioglu, K.H., Giesen, R.H., Morlighem, M., 2017. Simulating the evolution of Hardangerjøkulen ice cap in southern Norway since the mid-Holocene and its sensitivity to climate change. Cryosphere 11, 281–302.
Åkesson, H., Nisancioglu, K.H., Nick, F.M., 2018a. Impact of fjord geometry on grounding line stability. Front. Earth Sci. 6, 1–17. https://doi.org/10.3389/feart.2018.00071.
Åkesson, H., Morlighem, M., Nisancioglu, K.H., Svendsen, J.J., Mangerud, J., 2018b. Atmosphere-driven ice sheet mass loss paced by topography: insights from modelling the south-western Scandinavian Ice Sheet. Quat. Sci. Rev. 195, 32–47. https://doi.org/10.1016/j.quascirev.2018.07.004.
Amap, 2017. Snow, Water, Ice and Permafrost in the Arctic (SWIPA); Summary for Policy-Makers. Technical Report Oslo, Norway.
Andersen, B.G., 1954. Randmorener i Sørvest-Norge. Norsk Geografisk Tidskrift 14, 273–342.
Andreassen, L.M., Elvehøy, H., Kjøllmoen, B., Engeset, R.V., Haakensen, N., 2005. Glacier mass-balance and length variation in Norway. Ann. Glaciol. 42, 317–325.
Andrews, J.T., 1975. Glacial Systems; an Approach to Glaciers and Their Environments. Technical Report.
Anundsen, K., Simonsen, A., 1967. Et pre-borealt breframstøt på Hardangervidda og i området mellom Bergensbanen og Jotunheimen. Årbok for Universitetet i Bergen. Matematisk-naturvitenskapelige serie 7, 1e42.
Aschwanden, Andy, Fahnestock, Mark A., Truffer, Martin, Brinkerhoff, Douglas, J., Hock, Regine, Khroulev, Constantine, Mottram, Ruth, Khan, S Abbas, 2019. Contribution of the Greenland Ice Sheet to sea level over the next millennium. Science advances 5 (6), eaav9396.
Bakke, J., Lie, Ø., Heegaard, E., Dokken, T., Haug, G.H., Birks, H.H., Dulski, P., Nilsen, T., 2009. Rapid oceanic and atmospheric changes during the Younger Dryas cold period. Nat. Geosci. 2, 202.
Bassis, J.N., Walker, C.C., 2012. Upper and lower limits on the stability of calving glaciers from the yield strength envelope of ice. Proc. Roy. Soc. Lond.: Mathematical, Physical and Engineering Sciences 468, 913–931. https://doi.org/10.1098/rspa.2011.0422.
Bassis, J.N., Petersen, S.V., Mac Cathles, L., 2017. Heinrich events triggered by ocean forcing and modulated by isostatic adjustment. Nature 542, 332–334.
Benn, D.I., Lehmkuhl, F., 2000. Mass balance and equilibrium-line altitudes of glaciers in high-mountain environments. Quat. Int. 65, 15–29.
Benn, D.I., Warren, C.R., Mottram, R.H., 2007. Calving processes and the dynamics of calving glaciers. Earth Sci. Rev. 82, 143–179.
Benn, D.I., Åström, J., Zwinger, T., Todd, J., Nick, F.M., Cook, S., Hulton, N.R.J., Luckman, A., 2017. Melt-under-cutting and buoyancy-driven calving from tidewater glaciers: new insights from discrete element and continuum model simulations. J. Glaciol. 63 (240), 691–702.
Birks, H.H., Battarbee, R.W., Birks, H., 2000. The development of the aquatic ecosystem at Kråkenes Lake, western Norway, during the late glacial and early Holocene-a synthesis. J. Paleolimnol. 23, 91–114.
Birks, H.H., Kristensen, D.K., Dokken, T.M., Andersson, C., 2005. Exploratory comparisons of quantitative temperature estimates over the last deglaciation in Norway and the Norwegian Sea. The Nordic Seas: An Integrated Perspective 341–355.
Bjune, A.E., Bakke, J., Nesje, A., Birks, H.J.B., 2005. Holocene mean July temperature and winter precipitation in western Norvay inferred from palynological and glaciological lake-sediment proxies. Holocene 15, 177–189, 10.1191/0959683605hl798rp.
Briner, J.P., Bini, A.C., Anderson, R.S., 2009. Rapid early Holocene retreat of a Laurentide outlet glacier through an Arctic fjord. Nat. Geosci. 2, 496–499.
Brondex, J., Gagliardini, O., Gillet-Chaulet, F., Durand, G., 2017. Sensitivity of grounding line dynamics to the choice of the friction law. J. Glaciol. 63 (241), 854–866.
Brown, R.J.E., 1960. The distribution of permafrost and its relation to air temperature in Canada and the USSR. Arctic 13, 163–177.
Catania, G.A., Stearns, L.A., Moon, T.A., Enderlin, E.M., Jackson, R.H., 2020. Future evolution of Greenland's marine-terminating outlet glaciers. J. Geophys. Res.: Earth Surface 125 (2).
Choi, Y., Morlighem, M., Wood, M., Bondzio, J.H., 2018. Comparison of four calving laws to model Greenland outlet glaciers. Cryosphere 12 (12).
Christensen, J., Kumar, K.K., Aldrian, E., An, S.-I., dnM deCastro, I.C., Dong, W., Goswami, P., Hall, A., Kanyanga, J., Kitoh, A., Kossin, J., Lau, N.-C., Renwick, J., Stephenson, D., Xie, S.-P., Zho, T., 2013. Climate Phenomena and Their Relevance for Future Regional Climate Change. Chapter Climate Change 2013: the Physical Sci- Ence Basis. Contribution of Working Group I to the Fifth Assessment Report of the Intergovernmental Panel on Climate Change. Cambridge University Press, Cambridge, United Kingdom and New York, NY, USA.
Cuffey, K.M., Paterson, W.S.B., 2010. The Physics of Glaciers. Elsevier.
Dokken, T., Andersson, C., Risebrobakken, B., 2015. Relative Abundance of Planktic Foraminifera and Calculated SSTs and SST Anomaly (11.1-25.5 Ka BP) in Sediment Core MD95-2010. https://doi.org/10.1594/PANGAEA.841922, 10.1594/PANGAEA.841922.
Eldevik, T., Risebrobakken, B., Bjune, A.E., Andersson, C., Birks, H.J.B., Dokken, T.M., Drange, H., Glessmer, M.S., Li, C., Nilsen, J.E.Ø., et al., 2014. A brief history of climate–the northern seas from the Last Glacial Maximum to global warming. Quat. Sci. Rev. 106, 225–246.
Fettweis, X., Franco, B., Tedesco, M., Van Angelen, J., Lenaerts, J., Van Den Broeke, M., Gallée, H., 2013. Estimating the Greenland ice sheet surface mass balance contribution to future sea level rise using the regional atmospheric climate model MAR. Cryosphere 7, 469–489.
Follestad, B.A., 1972. The deglaciation of the south-western part of the Folgefonn peninsula, Hordaland. Norges geologiske Undersøkelser 280, 31–64.
Førre, E., 2012. Topografi Og Dreneringsretninger under Nordfonna, Folgefonna. Master's thesis. The University of Bergen.
Fowler, A., 2010. Weertman, Lliboutry and the development of sliding theory. J. Glaciol. 56, 965–972.
Gomez, N., Mitrovica, J.X., Huybers, P., Clark, P.U., 2010. Sea level as a stabilizing factor for marine-ice-sheet grounding lines. Nat. Geosci. 3, 850.
Hamborg, M., Mangerud, J., 1981. En rekonstruksjon av isbevegelser under siste istid i Samnanger og Kvam, Hordaland, Vest-Norge. Norges geologiske undersøkelse 369, 77–98.
Hanna, E., Huybrechts, P., Cappelen, J., Steffen, K., Bales, R.C., Burgess, E., McConnell, J.R., Peder Steffensen, J., Van den Broeke, M., Wake, L., et al., 2011. Greenland Ice Sheet surface mass balance 1870 to 2010 based on Twentieth Century Reanalysis, and links with global climate forcing. J. Geophys. Res.: Atmosphere 116.
Hanson, B., Hooke, R.L., 2000. Glacier calving: a numerical model of forces in the calving- speed–water-depth relation. J. Glaciol. 46, 188–196.

Harrison, W., Elsberg, D., Echelmeyer, K., Krimmel, R., 2001. On the characterization of glacier response by a single time-scale. J. Glaciol. 47, 659–664.
Haseloff, M., Sergienko, O.V., 2018. The effect of buttressing on grounding line dynamics. J. Glaciol. 64, 417–431.
Holland, D.M., Thomas, R.H., De Young, B., Ribergaard, M.H., Lyberth, B., 2008. Acceleration of Jakobshavn Isbrae triggered by warm subsurface ocean waters. Nat. Geosci. 1, 659–664.
Holtedahl, H., 1975. The Geology of the Hardangerfjord, West Norway. Universitetsforlaget.
Howat, I.M., Joughin, I., Tulaczyk, S., Gogineni, S., 2005. Rapid retreat and acceleration of Helheim Glacier, east Greenland. Geophys. Res. Lett. 32 (22).
Howat, I.M., Eddy, A., 2011. Multi-decadal retreat of Greenland's marine-terminating glaciers. J. Glaciol. 57, 389–396.
Hughes, A.L., Gyllencreutz, R., Lohne, Ø.S., Mangerud, J., Svendsen, J.I., 2016. The last Eurasian ice sheets–a chronological database and time-slice reconstruction, DATED-1. Boreas 45, 1–45.
Hughes, A.L., Rainsley, E., Murray, T., Fogwill, C.J., Schnabel, C., Xu, S., 2012. Rapid response of Helheim Glacier, southeast Greenland, to early Holocene climate warming. Geology 40, 427–430.
Huss, M., Farinotti, D., 2012. Distributed ice thickness and volume of all glaciers around the globe. J. Geophys. Res.: Earth Surface 117.
Jamieson, S.S., Vieli, A., Livingstone, S.J., Cofaigh, C.Ó., Stokes, C., Hillenbrand, C.-D., Dowdeswell, J.A., 2012. Ice-stream stability on a reverse bed slope. Nat. Geosci. 5, 799–802.
Jenkins, A., 2011. Convection-driven melting near the grounding lines of ice shelves and tidewater glaciers. J. Phys. Oceanogr. 41 (12), 2279–2294.
Joughin, I., Howat, I., Alley, R.B., Ekstrom, G., Fahnestock, M., Moon, T., Nettles, M., Truffer, M., Tsai, V.C., 2008. Ice-front variation and tidewater behavior on Helheim and kangerdlugssuaq glaciers, Greenland. J. Geophys. Res.: Earth Surface 2003–2012, 113.
Kajanto, K., Seroussi, H., de Fleurian, B., Nisancioglu, K.H., 2020. Present day Jakobshavn Isbræ close to the Holocene minimum extent. Quat. Sci. Rev. 246, 106492.
Kartverket (Norwegian Mapping Authority), 2017. Bathymetry Database Product "Dybdedata - Terrengmodeller 50 Meters Grid through. https://kartkatalog.geonorge.no/metadata/dybdedata-raadata/, 2017-8-11.
Khazendar, A., Fenty, I.G., Carroll, D., Gardner, A., Lee, C.M., Fukumori, I., Want, O., Zhang, H., Seroussi, H., Moller, D., Noël, B.P., van den Broeke, M.R., Dinardo, S., Willis, J., 2019. Interruption of two decades of Jakobshavn Isbrae acceleration and thinning as regional ocean cools. Nat. Geosci. 12 (4), 277–283.
Lichtenecker, N., 1936. Die gegenwärtige und die eiszeitliche Schneegrenze in den Os- talpen. In: Verhandl. D. III. Intern. Quart~ Ir-Konferenz Wien, pp. 141–147.
Lohne, Ø.S., Mangerud, J., Svendsen, J.I., 2012. Timing of the Younger Dryas glacial maximum in western Norway. Journal of Quaternary Science 27 (1), 81–88.
Luckman, A., Murray, T., De Lange, R., Hanna, E., 2006. Rapid and synchronous ice-dynamic changes in East Greenland. Geophys. Res. Lett. 33.
Luthi, M., Funk, M., Iken, A., Gogineni, S., Truffer, M., 2002. Mechanisms of fast flow in Jakobshavn Isbrae, West Greenland: Part III. Measurements of ice deformation, temperature and cross-borehole conductivityin boreholes to the bedrock. J. Glaciol. 48, 369–385.
Mangerud, J., 1987. The allerød/younger Dryas boundary. In: Berger, W.H., Labeyrie, L.D. (Eds.), Abrupt Climatic Change – Evidence and Implications, vol. 1987. D. Reidel, pp. 163–171.
Mangerud, J., Aarseth, I., Hughes, A.L., Lohne, Ø.S., Sk År, K., Sønstegaard, E., Svendsen, J.I., 2016. A major re-growth of the scandinavian ice sheet in western Norway during allerød-younger Dryas. Quat. Sci. Rev. 132, 175–205.
Mangerud, J., Goehring, B.M., Lohne, Ø.S., Svendsen, J.I., Gyllencreutz, R., 2013. Collapse of marine-based outlet glaciers from the scandinavian ice sheet. Quat. Sci. Rev. 67, 8–16.
Mangerud, J., Hughes, A.L., Sæle, T.H., Svendsen, J.I., 2019. Ice-flow patterns and precise timing of ice sheet retreat across a dissected fjord landscape in western Norway. Quat. Sci. Rev. 214, 139–163.
Mangerud, J., Svendsen, J.I., 2018. The Holocene thermal maximum around Svalbard, Arctic North Atlantic; molluscs show early and exceptional warmth. The Holocene 28 (1), 65–83.
Moon, T., Joughin, I., Smith, B., Howat, I., 2012. 21st-century evolution of Greenland outlet glacier velocities. Science 336, 576–578.
Morlighem, M., Wood, M., Seroussi, H., Choi, Y., Rignot, E., 2019. Modeling the response of northwest Greenland to enhanced ocean thermal forcing and subglacial discharge. Cryosphere 13 (2).
Murray, T., Scharrer, K., James, T., Dye, S., Hanna, E., Booth, A., Selmes, N., Luckman, A., Hughes, A., Cook, S., et al., 2010. Ocean regulation hypothesis for glacier dynamics in southeast Greenland and implications for ice sheet mass changes. J. Geophys. Res.: Earth Surface 115.
Nias, I.J., Cornford, S.L., Edwards, T.L., Gourmelen, N., Payne, A.J., 2019. Assessing uncertainty in the dynamical ice response to ocean warming in the Amundsen Sea Embayment, West Antarctica. Geophys. Res. Lett. 46 (20), 11253–11260.
Nick, F.M., Vieli, A., Howat, I.M., Joughin, I., 2009. Large-scale changes in Greenland outlet glacier dynamics triggered at the terminus. Nat. Geosci. 2 (2), 110–114.
Nick, F., Van der Veen, C., Vieli, A., Benn, D., 2010. A physically based calving model applied to marine outlet glaciers and implications for the glacier dynamics. J. Glaciol. 56, 781–794.
Nick, F.M., Vieli, A., Andersen, M.L., Joughin, I., Payne, A., Edwards, T.L., Pattyn, F., van de Wal, R.S., 2013. Future sea-level rise from Greenland's main outlet glaciers in a warming climate. Nature 497, 235–238.
Nye, J., 1951. The flow of glaciers and ice-sheets as a problem in plasticity. In: Proceedings of the Royal Society of London A: Mathematical, Physical and Engineering Sciences, vol. 207. The Royal Society, pp. 554–572.
Nye, J., 1952. The mechanics of glacier flow. J. Glaciol. 2, 82–93.
Nye, J.F., 1953. The flow law of ice from measurements in glacier tunnels, laboratory experiments and the Jungfraufirn borehole experiment. Proc. Roy. Soc. Lond. Math. Phys. Sci. 219, 477–489.
O'Leary, M., Christoffersen, P., 2013. Calving on tidewater glaciers amplified by submarine frontal melting. Cryosphere 7, 119.
Paterson, W., 1994. The Physics of Glaciers. Butterworth-Heinemann.
Pollard, D., DeConto, R.M., Alley, R.B., 2015. Potential Antarctic Ice Sheet retreat driven by hydrofracturing and ice cliff failure. Earth Planet Sci. Lett. 412, 112–121.
Pelto, M.S., Warren, C.R., 1991. Relationship between tidewater glacier calving velocity and water depth at the calving front. Ann. Glaciol. 15, 115–118.
Raup, B.H., Racoviteanu, A., Khalsa, S.J.S., Helm, C., Armstrong, R., Arnaud, Y., 2007. The GLIMS geospatial glacier database: a new tool for studying glacier change. Global Planet. Change 56, 101–110. https://doi.org/10.1016/j.gloplacha.2006.07.018.
Rea, B.R., Evans, D.J., 2007. Quantifying climate and glacier mass balance in north Norway during the Younger Dryas. Palaeogeogr. Palaeoclimatol. Palaeoecol. 246, 307–330.
Rignot, E., Steffen, K., 2008. Channelized bottom melting and stability of floating ice shelves. Geophys. Res. Lett. 35.
Ritz, C., Edwards, T.L., Durand, G., Payne, A.J., Peyaud, V., Hindmarsh, R.C., 2015. Potential sea-level rise from Antarctic ice-sheet instability constrained by observations. Nature 528 (7580), 115–118.
Roe, G.H., O'Neal, M.A., 2009. The response of glaciers to intrinsic climate variability: observations and models of late-Holocene variations in the Pacific Northwest. J. Glaciol. 55 (193), 839–854.
Rosenau, R., Schwalbe, E., Maas, H.-G., Baessler, M., Dietrich, R., 2013. Grounding line migration and high-resolution calving dynamics of Jakobshavn Isbræ, West Greenland. J. Geophys. Res. Earth Surf. 118, 382–395. https://doi.org/10.1029/2012JF002515.
Romundset, A., Lohne, Ø.S., Mangerud, J., Svendsen, J.I., 2010. The first Holocene relative sea-level curve from the middle part of Hardangerfjorden, western Norway. Boreas 39, 87–104.
Schoof, C., 2007. Ice sheet grounding line dynamics: steady states, stability, and hysteresis. J. Geophys. Res.: Earth Surface 112. https://doi.org/10.1029/2006JF000664 n/a–n/a, 10.1029/2006JF000664.
Schoof, C., Davis, A.D., Popa, T.V., 2017. Boundary layer models for calving marine outlet glaciers. Cryosphere 11, 2283–2303.
Simonsen, S.B., Johnsen, S., Popp, T., Vinther, B., Gkinis, V., Steen-Larsen, H., 2011. Past surface temperatures at the NorthGRIP drill site from the difference in firn diffusion of water isotopes. Clim. Past 7, 1327.
Slater, D.A., Goldberg, D.N., Nienow, P.W., Cowton, T.R., 2016. Scalings for submarine melting at tidewater glaciers from buoyant plume theory. J. Phys. Oceanogr. 46, 1839–1855.
Slater, D.A., Straneo, F., Felikson, D., Little, C.M., Goelzer, H., Fettweis, X., Holte, J., 2019. Estimating Greenland tidewater glacier retreat driven by submarine melting. Cryosphere 13, 2489–2509. https://doi.org/10.5194/tc-13-2489-2019.
Sole, A., Nienow, P., Bartholomew, I., Mair, D., Cowton, T., Tedstone, A., King, M.A., 2013. Winter motion mediates dynamic response of the Greenland ice sheet to warmer summers. Geophys. Res. Lett. 40, 3940–3944.
Steffensen, J.P., Andersen, K.K., Bigler, M., Clausen, H.B., Dahl-Jensen, D., Fischer, H., Goto-Azuma, K., Hansson, M., Johnsen, S.J., Jouzel, J., et al., 2008. High- resolution Greenland ice core data show abrupt climate change happens in few years. Science 321, 680–684.
Steiger, N., Nisancioglu, K.H., Åkesson, H., Fleurian, B.d., Nick, F.M., 2018. Simulated retreat of Jakobshavn Isbræ since the Little ice age controlled by geometry. Cryosphere 12, 2249–2266.
Stocker, T.F., Dahe, Q., Plattner, G.-K., 2013. Climate Change 2013: the Phys- Ical Science Basis. Working Group I Contribution to the Fifth Assessment Report of the Intergovernmental Panel on Climate Change. Summary for Policymakers (IPCC, 2013).
Stokes, C.R., Corner, G.D., Winsborrow, M.C., Husum, K., Andreassen, K., 2014. Asynchronous response of marine-terminating outlet glaciers during deglaciation of the Fennoscandian Ice Sheet. Geology 42, 455–458.
Straneo, F., Heimbach, P., 2013. North Atlantic warming and the retreat of Greenland's outlet glaciers. Nature 504, 36.
Streuff, K., Cofaigh, C.Ó., Hogan, K., Jennings, A., Lloyd, J.M., Noormets, R., Nielsen, T., Dowdeswell, J.A., Weinrebe, W., 2017. Seafloor geomorphology and glacimarine sedimentation associated with fast-flowing ice sheet outlet glaciers in Disko Bay, West Greenland. Quat. Sci. Rev. 169, 206–230.
Van Beusekom, A.E., O'Nell, S.R., March, R.S., Sass, L.C., Cox, L.H., 2010. Re- analysis of Alaskan benchmark glacier mass-balance data using the index method. Technical Report US Geological Survey.
Van der Veen, C.J., Whillans, I., 1996. Model experiments on the evolution and stability of ice streams. Ann. Glaciol. 23, 129–137.
Vieli, A., Funk, M., Blatter, H., 2001. Flow dynamics of tidewater glaciers: a numerical modelling approach. J. Glaciol. 47, 595–606.
Vieli, A., Payne, A., 2005. Assessing the ability of numerical ice sheet models to simulate grounding line migration. J. Geophys. Res.: Earth Surface 2003–2012, 110.
Vieli, A., Nick, F.M., 2011. Understanding and modelling rapid dynamic changes of

tidewater outlet glaciers: issues and implications. Surv. Geophys. 32 (4–5), 437–458.
Van de Wal, R., Greuell, W., van den Broeke, M.R., Reijmer, C., Oerlemans, J., 2005. Surface mass-balance observations and automatic weather station data along a transect near Kangerlussuaq, West Greenland. Ann. Glaciol. 42, 311–316.
Van de Wal, R., Boot, W., Van den Broeke, M., Smeets, C., Reijmer, C., Donker, J., Oerlemans, J., 2008. Large and rapid melt-induced velocity changes in the ablation zone of the Greenland Ice Sheet. Science 321, 111–113.
Walter, F., O'Neel, S., McNamara, D., Pfeffer, W., Bassis, J.N., Fricker, H.A., 2010. Iceberg calving during transition from grounded to floating ice: columbia Glacier, Alaska. Geophys. Res. Lett. 37.
Weertman, J., 1964. The theory of glacier sliding. J. Glaciol. 5, 287–303. https://doi.org/10.1007/978-1-349-15480-7_14.
Weertman, J., 1974. Stability of the junction of an ice sheet and an ice shelf. J. Glaciol. 13, 3–11.
Young, N.E., Briner, J.P., Stewart, H.A., Axford, Y., Csatho, B., Rood, D.H., Finkel, R.C., 2011. Response of Jakobshavn Isbræ, Greenland, to Holocene climate change. Geology 39, 131–134.